The Astronomical Journal, 133:2020–2036, 2007 May

THE 2004–2006 OUTBURST AND ENVIRONMENT OF V1647 ORI

J. A. Acosta-Pulido
Instituto de Astrofísica de Canarias, E-38200 La Laguna, Tenerife, Canary Islands, Spain; jap@iac.es

M. Kun, P. Ábrahám, Á. Kóspál, and Sz. Csizmadia
Konkoly Observatory, H-1525 Budapest, Hungary

L. L. Kiss[1]
School of Physics, University of Sydney, Sydney, NSW, Australia

A. Moór, L. Szabados, and J. M. Benkő
Konkoly Observatory, H-1525 Budapest, Hungary

R. Barrena Delgado and M. Charcos-Llorens[2]
Instituto de Astrofísica de Canarias, E-38200 La Laguna, Tenerife, Canary Islands, Spain

M. Eredics
Konkoly Observatory, H-1525 Budapest, Hungary

Z. T. Kiss
Baja Astronomical Observatory, H-6500 Baja, Hungary

A. Manchado[3]
Instituto de Astrofísica de Canarias, E-38200 La Laguna, Tenerife, Canary Islands, Spain

M. Rácz
Konkoly Observatory, H-1525 Budapest, Hungary

C. Ramos Almeida
Instituto de Astrofísica de Canarias, E-38200 La Laguna, Tenerife, Canary Islands, Spain

P. Székely
Department of Experimental Physics and Astronomical Observatory, University of Szeged, H-6720 Szeged, Hungary

and

M. J. Vidal-Núñez[4]
Instituto de Astrofísica de Canarias, E-38200 La Laguna, Tenerife, Canary Islands, Spain
Received 2006 October 4; accepted 2006 December 14

ABSTRACT

We studied the brightness and spectral evolution of the young eruptive star V1647 Ori during its recent outburst in the period 2004 February–2006 September. We performed a photometric follow-up in the bands V, R_C, I_C, J, H, and K_s, as well as visible and near-IR spectroscopy. The main results derived from combining our data with those published by other authors are as follows: the brightness of V1647 Ori stayed more than 4 mag above the preoutburst level until 2005 October, when it started a rapid fading. In the high state we found a periodic component in the optical light curves with a period of 56 days. The delay between variations of the star and variations in the brightness of clumps of nearby nebulosity corresponds to an angle of $61^\circ \pm 14^\circ$ between the axis of the nebula and the line of sight. The overall appearance of the infrared and optical spectra did not change in the period 2004 March–2005 March, although a steady decrease of H I emission-line fluxes could be observed. In 2006 May, in the quiescent phase, the He I 1.083 μm line was observed in emission, contrary to its deep blueshifted absorption observed during the outburst. The $J - H$ and $H - K_s$ color maps of the infrared nebula reveal an envelope around the star whose largest extension is about $18''$ (0.03 pc). The color distribution of the infrared nebula suggests reddening of the scattered light inside a thick circumstellar disk. Comparison of the K_s and Hα images of McNeil's Nebula, the conical nebulosity illuminated by V1647 Ori, shows that HH 22A, the *Spitzer* infrared source, and the bright clump C of the nebula may be unrelated objects. We show that the observed properties of V1647 Ori could be interpreted in the framework of the thermal instability models of Bell and coworkers. V1647 Ori might belong to a new class of young eruptive stars, defined by relatively short timescales, recurrent outbursts, a modest increase in bolometric luminosity and accretion rate, and an evolutionary state earlier than that of typical EXors.

Key words: circumstellar matter — ISM: individual (McNeil's Nebula) — stars: formation — stars: individual (V1647 Ori) — stars: pre–main-sequence

Online material: color figures

[1] On leave from University of Szeged, H-6720 Szeged, Hungary.
[2] Department of Astronomy, University of Florida, Gainesville, FL 32611, USA.
[3] Consejo Superior de Investigaciones Cientificas, E-28006 Madrid, Spain.
[4] Instituto de Astrofísica de Andalucía, E-18080 Granada, Spain.

1. INTRODUCTION

Eruptive young stellar objects form a small but spectacular class of pre-main-sequence stars. Traditionally, they are divided into two groups. FU Orionis–type stars (FUors) are characterized by an initial brightening of ~5 mag during several months or years, followed by a fading phase of up to several decades or a century. Their spectral type is F–G giant according to the optical spectrum, and K–M giant/supergiant at near-infrared (NIR) wavelengths. The second group, called EX Lupi–type stars (EXors), belongs to the T Tauri class. Their recurrent outbursts are relatively short, lasting from some weeks to months, and the time between the eruptions ranges from months to years. Their spectral type is K or M dwarf.

The recent outburst of the young star V1647 Ori offered a rare opportunity to study phenomena accompanying the eruption of a low-mass pre-main-sequence star. Following a 3 month brightening of $\Delta I_C \sim 4.5$ mag (Briceño et al. 2004), V1647 Ori reached peak light in 2004 January, illuminating also a conical reflection nebulosity called McNeil's Nebula (McNeil 2004). The object stayed in high state for about 2 yr, then started a rapid fading in 2005 October (Kóspál et al. 2005). V1647 Ori already exhibited a similar eruption in 1966–1967 (Aspin et al. 2006).

During the 2004–2005 outburst V1647 Ori was intensively studied from many aspects. The brightness evolution at optical and NIR wavelengths was monitored by Briceño et al. (2004), Reipurth & Aspin (2004), Walter et al. (2004), McGehee et al. (2004), and Ojha et al. (2005, 2006). The optical/infrared spectrum and its changes were studied by Vacca et al. (2004), Walter et al. (2004), Andrews et al. (2004), Rettig et al. (2005), Ojha et al. (2006), and Gibb et al. (2006). The structure of the circumstellar matter and the physics of the outburst were investigated by McGehee et al. (2004), Muzerolle et al. (2005), and Rettig et al. (2005). The X-ray properties of the star were studied by Grosso et al. (2005) and Kastner et al. (2004, 2006). These works produced a wealth of very important information on the eruption, but a general picture is still to be worked out. Nevertheless, all authors seem to agree that V1647 Ori is a deeply embedded low-mass pre-main-sequence object; it is surrounded by a disk; the outburst was caused by increased accretion; and the eruption was accompanied by strong stellar wind. It is still an open question whether V1647 Ori belongs to the FUor or the EXor class, and whether the standard outburst models, developed for FU Ori events, could be applied for this case (or how they should be modified to make them applicable).

In this paper we present and analyze the results of our monitoring program on V1647 Ori. The data, which include optical (V, R_C, and I_C) and NIR (J, H, and K_s) imaging, and intermediate-resolution optical and NIR spectroscopic observations, were obtained between 2004 February and 2006 May, covering the whole outburst period. Following a description of the observations and data reduction (§ 2), in § 3 we present results on the photometric evolution of V1647 Ori. Sections 4 and 5 are devoted to the spectroscopic variability and the morphology of the nebula, respectively. In § 6 we discuss the physics of the outburst, and comment on the FUor-or-EXor question. Our results are briefly summarized in § 7.

2. OBSERVATIONS AND DATA REDUCTION

2.1. *Optical Imaging and Photometry*

Optical observations of V1647 Ori were obtained on 45 nights in the period 2004 February 12–2006 February 1. The measurements were performed in two observatories with three telescopes: the IAC-80 telescope of the Teide Observatory (Spain), and the 1 m Ritchey-Chrétien-Coudé (RCC) and 60/90/180 cm Schmidt telescopes of the Konkoly Observatory (Hungary).

The IAC-80 telescope was equipped with a 1024×1024 Thomson CCD with a scale of $0.4325''$ pixel^{-1} and a field of view of $7.4' \times 7.4'$. For the broadband *VRI* observations we used the IAC#72, IAC#71, and IAC#70 filters.[5] Typically, three frames were taken with exposure times of 120–300 s frame^{-1} each night. In addition, on the night of 2004 January 11 deep Hα and [S II] images were obtained using the narrowband filters IAC#17 and IAC#68. Four exposures of 1200 s were taken through each filter.

At Konkoly Observatory, the 1 m RCC telescope was equipped with a Princeton Instruments VersArray 1300B camera. The back-illuminated 1340×1300 CCD has an image scale of $0.306''$ pixel^{-1} and a field of view of $6.8' \times 6.6'$. The Schmidt telescope was equipped with a 1536×1024 Kodak Photometrics AT 200 CCD camera. The image scale was $1.03''$ pixel^{-1}, providing a field of view of $24' \times 17'$. On both telescopes, the $V(RI)_C$ filters used matched closely the standard Johnson-Cousins system (Hamilton et al. 2005). For each filter, 3–10 frames were taken on each night, and the integration times varied between 120 and 600 s frame^{-1}.

2.1.1. *Data Reduction and Photometric Calibration*

Raw frames were dark-subtracted and flat-fielded using the `imred` package within the IRAF[6] environment. Dome flat-field images were taken each night, and sometimes sky flats were also available. In some cases, the consecutive frames taken through the same filter were co-added in order to increase the signal-to-noise ratio (S/N). As an example, Figure 1 shows *R*-band optical images of V1647 Ori taken with the 1 m RCC telescope of the Konkoly Observatory at three different phases of the outburst. The narrowband Hα and [S II] images were bias-subtracted, flat-fielded, and combined per filter. Then a scaled *R*-band image, assumed to be a proper continuum, was subtracted from them in order to show the pure emission-line map.

The instrumental $V(RI)_C$ magnitudes of V1647 Ori were determined by point-spread function (PSF) photometry using the DAOPHOT package in IRAF (Stetson 1987). The field of view of our telescopes allowed us to include several field stars to define the PSF of the images. The use of PSF photometry was important to exclude the contribution of the nebula, which becomes dominant especially in the *V* band. In order to assure the consistency of the results obtained with the three different telescopes, we treated our data in a homogeneous manner: the position and extension of the sky region near V1647 Ori were the same in all images, and the preliminary aperture photometry, used for scaling the PSF magnitudes, was obtained using equally narrow apertures ($1.5''$) in each image.

For photometric calibration we used the secondary standards from the list of Semkov (2006). Differential photometry was performed by computing the instrumental magnitude differences between V1647 Ori and each comparison star. The differential magnitudes were transformed into the standard photometric system as follows. For the comparison stars, we searched for a relationship between Δm, the differences between instrumental and absolute magnitudes in the V, R_C, or I_C band, and the color indices of the stars, similarly to as described in Serra-Ricart et al.

[5] The transmission curves are available at http://www.iac.es/telescopes/tcs/filtros-eng.htm.

[6] IRAF is distributed by the National Optical Astronomy Observatory, which is operated by the Association of Universities for Research in Astronomy, Inc., under cooperative agreement with the National Science Foundation (see http://iraf.noao.edu).

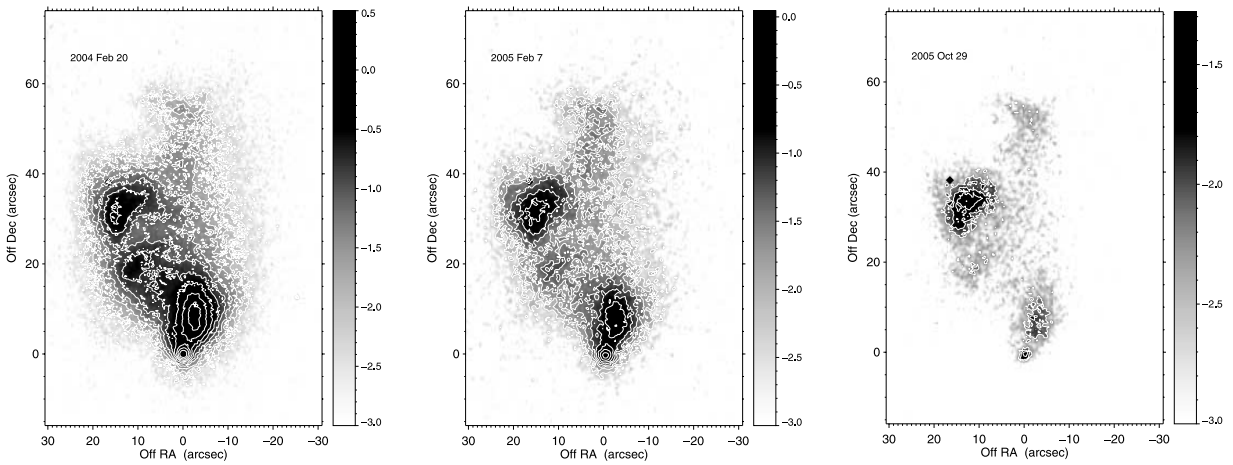

FIG. 1.—Examples of *R*-band optical images of V1647 Ori taken with the 1 m RCC telescope of the Konkoly Observatory at three different phases of the outburst. North is at the top, and east is to the left. V1647 Ori is located at the southern apex of the nebula. The color table has been scaled to represent the same brightness in all three images. [*See the electronic edition of the Journal for a color version of this figure*.]

(1999). We note that the color indices of the comparison stars covered a large enough range to bracket the color indices of V1647 Ori. The data points were fitted with a linear relationship, except a few low-quality nights, when due to large scatter all Δm values were averaged. For a given telescope, the derived color terms (the slope of the fit) were consistent from night to night within the formal uncertainties provided by the fitting procedure. Color terms computed from the 1 m RCC observations also agreed with values determined with high precision from observations of NGC 7790 with the same instrument. For calibration of the V1647 Ori data we applied the color terms determined for the corresponding night. Results of the optical photometry of V1647 Ori are presented in Table 1 and plotted in Figure 2. The uncertainties given in Table 1 were computed as the quadratic sum of the formal errors of the instrumental magnitudes provided by IRAF and the uncertainties of the standard transformation. In those cases for which the frames were evaluated separately (rather than co-added), the standard deviation of the magnitudes from each frame was also computed, and the maximum of the two types of errors was adopted.

2.2. *Near-Infrared Imaging, Photometry, and Polarimetry*

NIR *J*-, *H*-, and K_s-band observations were carried out at 10 epochs in the period 2004 March–2006 March. The data were obtained using two instruments: LIRIS, installed on the 4.2 m William Herschel Telescope (WHT) at the Observatorio del Roque de Los Muchachos; and CAIN-2, installed on the 1.52 m Telescope Carlos Sanchez (TCS) at the Teide Observatory. Table 2 lists the epochs of all NIR observations. In addition, polarization images through a *J* filter were obtained during the night of 2004 October 28, using the instrument LIRIS.

LIRIS is a NIR camera/spectrograph attached to the Cassegrain focus of the WHT (Acosta-Pulido et al. 2003; Manchado-Torres et al. 2003). The data were obtained during the commissioning period (2004 March), plus some nights corresponding to the guaranteed time of the instrument team. LIRIS is based on a Hawaii-I detector with an image scale of $0.25''$ pixel^{-1} and a $4.2' \times 4.2'$ field of view. Observations were always performed by taking several dithered exposures around the position of V1647 Ori in order to ensure proper sky-image subtraction. For each dither point we took several frames using a short exposure time to avoid saturation, which were later averaged to obtain the final reduced image. The minimum exposure time was 1 s for individual exposures; the total integration time per filter was about 5 minutes. During the first observing period the individual exposure times were optimized to detect the nebula, which nearly saturated the detector at the position of the illuminating star.

The infrared camera CAIN-2 at the 1.52 m TCS is equipped with a 256×256 Nicmos 3 detector, which provides a pixel projection of $1''$ with its wide optics configuration. The same dithering technique was used as in the case of LIRIS observations. Total integration time was usually 10 minutes in all filters (*J*, *H*, and K_s), split into many exposures of 0.5–3 s, the shortest corresponding to filter K_s and the longest to filter *J*.

2.2.1. *Data Reduction and Photometric Calibration*

The data reduction process involved the following steps: sky subtraction, flat-fielding, and the co-addition of all frames taken with the same filter. The sky image was obtained as the median combination of all frames, masking regions occupied by bright sources. The final image was produced using the standard "shift-and-add" technique, including rejection of outlier pixels. The LIRIS images were reduced using the package LIRIS_QL developed within the IRAF environment. The CAIN-2 data were also treated with IRAF tasks. The *J* and K_s images obtained on 2004 November 4 can be seen in Figure 3.

The instrumental magnitudes of the central star were extracted using aperture photometry, since the contribution of the nebula in the NIR becomes negligible compared to it. Based on the measured radial profiles, we estimate that the nebula contributes to the central star photometry at most 15% in the *J* band, but less than 5% in the K_s band. Due to the high brightness of V1647 Ori, some LIRIS images entered the nonlinear regime at the position of the star. In these cases we estimated the flux of the star by fitting a PSF model to the nonsaturated parts of the stellar profile using the DAOPHOT package in IRAF.

For the photometric calibration we used the Two Micron All Sky Survey (2MASS) catalog (Cutri et al. 2003). In general, five or six 2MASS stars were found within the sky region covered by our images. We have determined the offset between the instrumental and the calibrated 2MASS magnitudes by averaging all available stars, after removal of deviant sources (identified as likely variable stars by Semkov 2006). Results of the NIR photometry for V1647 Ori are listed in Table 2, and the light curves are shown in Figure 2. The standard deviation is used as an estimate of the measurement error and is reported in Table 2. We cannot determine a reliable color-term correction using our reduced number of reference stars. The 2MASS star J054611162−0006279 was always

TABLE 1
Optical Photometry of V1647 Ori

Date	JD[a]	V	R_C	I_C	Telescope
2004 Feb 12	048.3	...	...	14.33 ± 0.04	Schmidt
2004 Feb 20	056.3	...	17.01 ± 0.08	14.62 ± 0.04	RCC
2004 Mar 6	071.3	...	...	14.56 ± 0.04	RCC
2004 Apr 1	097.2	...	...	14.83 ± 0.08	Schmidt
2004 Apr 2	098.3	...	16.28 ± 0.08	14.51 ± 0.06	Schmidt
2004 Apr 24	120.3	18.92 ± 0.06	16.91 ± 0.04	14.73 ± 0.07	IAC-80
2004 Aug 31	248.6	19.00 ± 0.12	16.86 ± 0.10	15.13 ± 0.15	RCC
2004 Sep 1	249.6	...	...	14.89 ± 0.08	IAC-80
2004 Sep 2	250.6	19.58 ± 0.08	17.00 ± 0.08	...	IAC-80
2004 Sep 3	251.6	...	...	14.74 ± 0.04	RCC
2004 Sep 6	254.6	...	17.08 ± 0.03	14.90 ± 0.04	RCC
2004 Sep 7	255.6	19.32 ± 0.06	17.62 ± 0.08	14.95 ± 0.03	RCC
2004 Oct 6	284.7	18.91 ± 0.10	17.24 ± 0.06	...	IAC-80
2004 Oct 25	303.6	19.23 ± 0.10	17.50 ± 0.05	15.21 ± 0.06	IAC-80
2004 Nov 1	310.8	...	...	14.99 ± 0.04	IAC-80
2004 Nov 21	330.7	18.86 ± 0.08	17.08 ± 0.08	...	IAC-80
2004 Nov 24	334.5		16.91 ± 0.07	14.72 ± 0.03	RCC
2004 Nov 30	340.4	19.04 ± 0.06	17.16 ± 0.04	14.87 ± 0.04	RCC
2004 Dec 11	350.5	19.56 ± 0.08	17.60 ± 0.05	15.23 ± 0.06	RCC
2004 Dec 22	361.5	18.87 ± 0.11	17.24 ± 0.08	14.91 ± 0.05	RCC
2004 Dec 30	370.3	18.92 ± 0.05	17.24 ± 0.06	15.01 ± 0.05	RCC
2005 Jan 6	377.3	...	16.95 ± 0.06	14.79 ± 0.07	RCC
2005 Jan 10	381.3	18.74 ± 0.06	17.08 ± 0.08	14.91 ± 0.10	RCC
2005 Jan 11	382.3	...	17.04 ± 0.07	14.84 ± 0.07	RCC
2005 Jan 20	391.3	...	17.35 ± 0.06	...	IAC-80
2005 Feb 1	403.3	...	17.67 ± 0.04	15.34 ± 0.10	RCC
2005 Feb 5	407.3	...	17.43 ± 0.09	15.23 ± 0.05	RCC
2005 Feb 7	409.3	18.93 ± 0.09	17.48 ± 0.07	15.09 ± 0.05	RCC
2005 Mar 21	451.3	19.06 ± 0.07	17.18 ± 0.03	...	IAC-80
2005 Oct 4	648.5	20.35 ± 0.10	18.65 ± 0.06	16.00 ± 0.08	RCC
2005 Oct 5	649.5	20.43 ± 0.06	18.58 ± 0.04	16.14 ± 0.05	RCC
2005 Oct 9	653.6	...	...	16.39 ± 0.06	RCC
2005 Oct 10	654.6	...	...	16.16 ± 0.04	RCC
2005 Oct 15	659.7	...	...	16.03 ± 0.07	RCC
2005 Oct 19	663.6	...	...	16.29 ± 0.05	RCC
2005 Oct 28	672.6	21.34 ± 0.16	19.49 ± 0.08	17.02 ± 0.08	RCC
2005 Oct 31	674.6	21.55 ± 0.16	19.66 ± 0.05	17.17 ± 0.03	RCC
2005 Nov 1	675.6	21.75 ± 0.08	19.83 ± 0.04	17.30 ± 0.04	RCC
2005 Nov 17	692.5	...	...	17.55 ± 0.08	RCC
2005 Nov 19	694.6	...	...	17.70 ± 0.10	RCC
2005 Dec 8	713.4	...	...	17.88 ± 0.10	RCC
2005 Dec 10	715.4	...	...	17.95 ± 0.10	RCC
2005 Dec 11	716.4	...	...	17.63 ± 0.10	RCC
2005 Dec 13	718.5	...	...	17.84 ± 0.10	RCC
2006 Feb 1	768.3	...	...	19.49 ± 0.10	RCC

[a] 2,453,000+.

included as a comparison star, since it shows calibration offsets close to the average in all occasions (details of this target are given in the Appendix). We note that this source was the only comparison star used by Walter et al. (2004) for the photometric calibration of their NIR data. The colors of this star are very similar to those of V1647 Ori, which reduces the importance of color terms when determining the photometrical calibration.

2.2.2. *Polarimetry*

The polarization images were obtained thanks to a double Wollaston prism (WeDoWo; Oliva 1997), located in the LIRIS grism wheel. This device produces four different images on the detector from a rectangular field of 4×1 arcmin^2. Each image corresponds to a different linear polarization angle, namely, 0°, 90°, 45°, and 135°. After distortion correction, proper alignment, and the combination of these images, the degree and angle of linear polarization can be determined. For V1647 Ori and its nebula we obtained an exposure of about 1800 s, divided into individual frames of 15 s. A small dither pattern of three points was performed around the source, interleaved with measurements at an offset position in order to determine a proper sky emission, given the extension of the source. The data reduction process is very similar to that followed in normal imaging mode; the LIRIS_QL package was used. Images of the linear polarization degree are presented and discussed in § 5.3.

2.3. *Near-Infrared Spectroscopy*

NIR spectrograms of V1647 Ori were obtained using LIRIS at five different epochs, four of them during the first year of the outburst. Five spectra cover the wavelength interval 0.9–1.4 μm

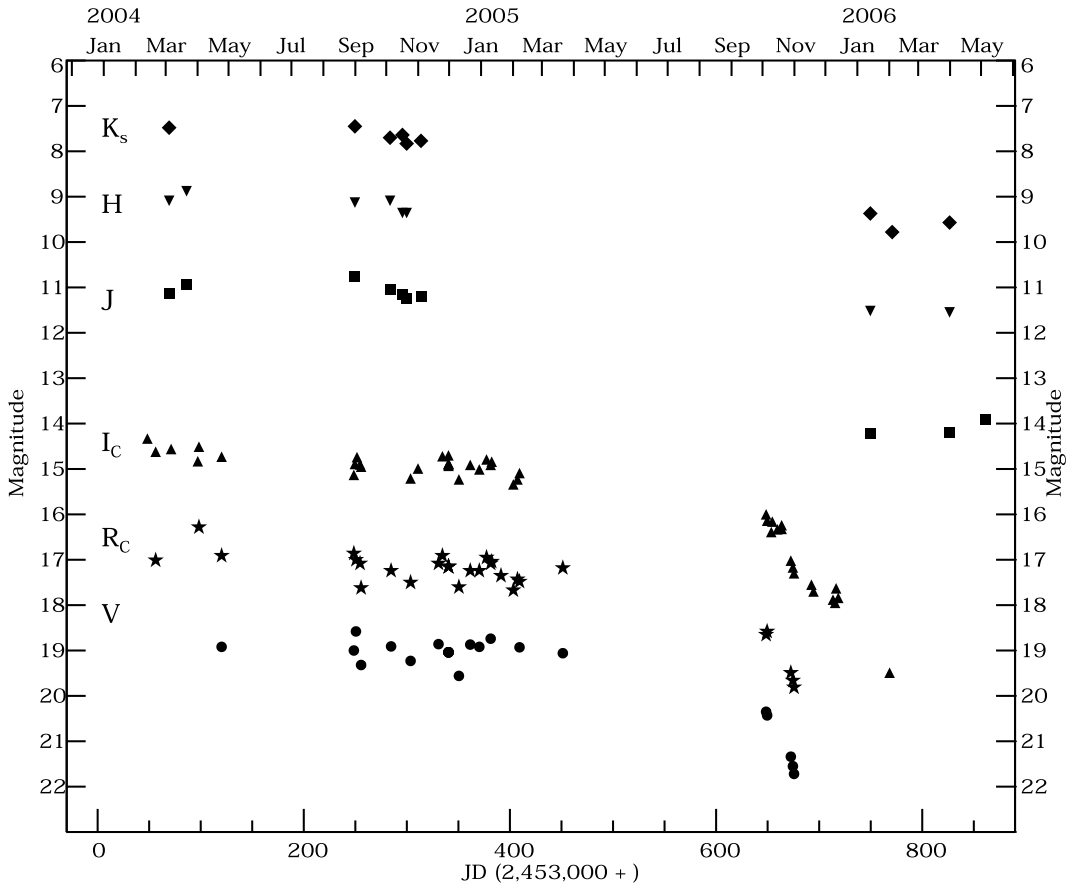

FIG. 2.— Light curves of V1647 Ori in the *V* (*circles*), R_C (*asterisks*), I_C (*upward triangles*), *J* (*squares*), *H* (*downward triangles*), and K_s (*diamonds*) bands between 2004 February 16 and 2006 May 5, based on the data presented in Tables 1 and 2. The uncertainties are comparable with symbol sizes.

(*ZJ* bands), and three others cover the 1.4–2.4 μm (*HK*) wavelength band. The log of the observations is presented in Table 3.

Observations were performed following an ABBA telescope nodding pattern in both the *ZJ* and *HK* bands. In order to reduce the readout noise, the measurements were done using multiple correlated readout mode, with four readouts before and after the integration. We used a slit width of 0.75″ or 1″, depending on the seeing conditions, which yielded a spectral resolution in the range $R = 500–660$ and 550–700 in the *ZJ* and *HK* spectra, respectively. The wavelength calibration was provided by observations of Argon and Xenon lamps available in the calibration unit at the A&G box of the telescope. In order to obtain the telluric correction and the flux calibration, nearby A0 V or G2 V stars were observed with the same configuration as the object.

The data were reduced and calibrated using the LIRIS_QL package. Consecutive pairs of AB two-dimensional images were subtracted to remove the sky background, then the resulting images were wavelength calibrated and flat-fielded before registering and co-adding all frames to provide the final combined spectrum. One-dimensional spectra were extracted with the IRAF `apall` task. The extracted spectra were divided by a composite spectrum to eliminate telluric contamination. This composite spectrum was

TABLE 2
NEAR-INFRARED PHOTOMETRY OF V1647 ORI

Date	JD[a]	*J*	*H*	K_s	Telescope
2004 Mar 4	069.4	11.13 ± 0.10	9.09 ± 0.07	7.48 ± 0.09	LIRIS
2004 Mar 21	086.3	11.00 ± 0.12	8.70 ± 0.19	...	TCS
2004 Sep 1	249.6	11.12 ± 0.10	9.17 ± 0.03	7.66 ± 0.01	TCS
2004 Oct 5	283.7	11.06 ± 0.07	9.07 ± 0.14	7.76 ± 0.05	TCS
2004 Oct 17	295.7	11.10 ± 0.09	9.09 ± 0.14	7.62 ± 0.04	TCS
2004 Oct 21	299.8	11.17 ± 0.08	9.19 ± 0.05	7.84 ± 0.08	TCS
2004 Nov 4	313.7	11.20 ± 0.06	...	7.77 ± 0.06	LIRIS
2006 Jan 14	749.6	14.27 ± 0.09	11.48 ± 0.08	9.41 ± 0.19	LIRIS
2006 Feb 6	770.8	...	...	9.78 ± 0.02	TCS
2006 Mar 31	826.5	14.19 ± 0.13	11.55 ± 0.05	9.57 ± 0.08	TCS
2006 May 5	861.4	13.92 ± 0.08	...	...	LIRIS
2006 Sep 9	987.8	...	11.59 ± 0.05	9.82 ± 0.06	LIRIS

[a] 2,453,000+.

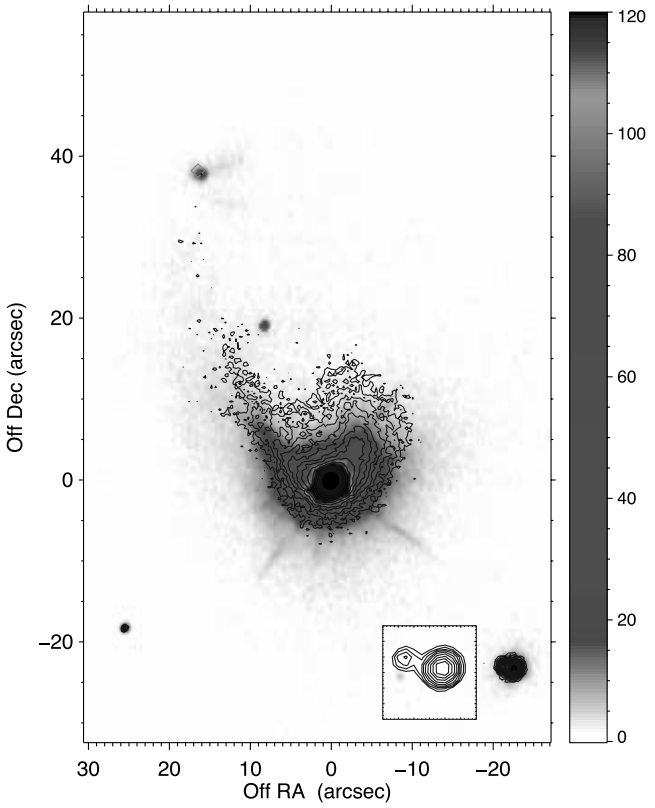

FIG. 3.—NIR images of McNeil's Nebula obtained on 2004 November 4 with LIRIS on WHT. North is at the top, and east is to the left. The color-scaled image represents the K_s-band emission, and the contours represent the J-band emission. The inset is a zoom of the star southwest of V1647 Ori, demonstrating that the star is a double system (see also the Appendix). The open diamond at $(\Delta\alpha, \Delta\delta) \simeq (16'', 38'')$ marks the position of the bright infrared source detected by Muzerolle et al. (2005) in *Spitzer* images. [*See the electronic edition of the Journal for a color version of this figure.*]

generated from the observed spectra of the calibration star, divided by a stellar model and convolved to our spectral resolution. We used the publicly available code Telluric (Vacca et al. 2003) to perform the correction when A0 stars were observed. Differences in the strength of telluric features are likely due to a mismatch of air masses, and the variation of atmospheric conditions between observations of the object and the reference star were taken into account using Beer's law. The IRAF task `telluric` was used in this step. The flux calibration was carried out normalizing to the J, H, and K_s magnitudes obtained in our NIR photometry. We show in Figure 4 the flux-calibrated infrared spectra for those observing dates when the full range from 0.9 to 2.4 μm was observed.

2.4. *Optical Spectroscopy*

Medium-resolution optical spectra were taken on three nights, 2004 October 28, November 1, and December 24, with the Double Beam Spectrograph mounted on the 2.3 m telescope of the Siding Spring Observatory (Australia). We used 1200 line mm^{-1} gratings in both arms of the spectrograph, while the exposure time was set to 20 minutes. The slit width was 2″, and the instrument's rotator kept it in the parallactic angle. The image scale was 0.9″ pixel^{-1} in the direction of the dispersion and 3.6″ pixel^{-1} perpendicular to it. The observed spectral ranges and resolutions were as follows: blue, 4800–5240 Å, $\lambda/\Delta\lambda = 8300$; red, 5820–6780 Å, $\lambda/\Delta\lambda = 6500$. All spectra were reduced with standard IRAF tasks, including bias and flat-field corrections, aperture extraction, and wavelength calibration.

TABLE 3
JOURNAL OF NEAR-INFRARED SPECTROSCOPY

Date	JD[a]	Slit (arcsec)	ZJ t_{exp} (s)	HK t_{exp} (s)	Air Mass
2004 Mar 8	073.4	1	400	12	1.3
2004 Nov 4	313.7	0.75	800	432	1.2
2005 Jan 24	395.4	0.75	200	...	1.2
2005 Mar 25	455.4	1	100	...	2.0
2006 May 5	861.4	1	1200	400	4.1
2006 Sep 9	987.7	0.75	1200	900	1.4

[a] 2,453,000+.

In the blue spectral range we observed a barely visible continuum, and could not detect the absorption spectrum observed by Briceño et al. (2004) in 2004 February. These blue spectra were excluded from further analysis. In the red range we observed the Hα emission line on a featureless continuum. The equivalent widths of the stellar Hα line determined from our observations are 32, 34, and 27 Å for the dates 2004 October 28, November 1, and December 24, respectively.

3. BRIGHTNESS VARIATIONS DURING THE V1647 ORI OUTBURST

3.1. *Long-Term Evolution*

In order to examine the flux evolution during the whole outburst history we combined our I_C measurements with those of Briceño et al. (2004), which covered the beginning of the eruption. The complete I_C-band light curve is displayed in Figure 5. Following an initial brightening of $\sim$4.5 mag between 2003 November and 2004 February (Briceño et al. 2004), the star faded only moderately during the next one and a half years. This gradual decrease of brightness was observable in all photometric bands with similar rates (Fig. 2). Then, between 2005 October and November the brightness of the star suddenly dropped by more than 1 mag at all optical wavelengths (Kóspál et al. 2005). This decay was also monitored by Semkov (2006) and Ojha et al. (2006). The rapid fading continued in the next months, although the rate was slightly slower after 2005 mid-November. By 2006 February, some 800 days after the onset of the eruption, V1647 Ori was very close to the reported preoutburst state.

The complete light curve of the outburst can naturally be divided into three phases: the initial rise, the "plateau," and the final decay. In order to quantify the rate of brightness evolution, we fitted straight lines to the data points in Figure 5 for each phase separately. The results are -1.3, 0.04, and 0.8 mag month^{-1}, respectively. It is remarkable that the pace of brightness change in the rising and decaying phases is similar.

The fact that the fading rate of V1647 Ori is apparently wavelength-independent is different from the case of another eruptive star V1057 Cyg, whose decline rate decreased monotonically from the ultraviolet to the mid-infrared during the years following the outburst (Kenyon & Hartmann 1991). However, the decline of V1057 Cyg was most pronounced in the B band, which was not observable in the case of V1647 Ori.

3.2. *A Periodicity of 56 Days*

The light curves in Figures 2 and 5 show that, in addition to the slow decline during the high plateau, short-timescale variations can be seen in each photometric band. Definite brightness minima can be recognized in each optical band, e.g., on 2004 December 10 (JD 2,453,350) and on 2005 February 1 (JD 2,453,403). Similar

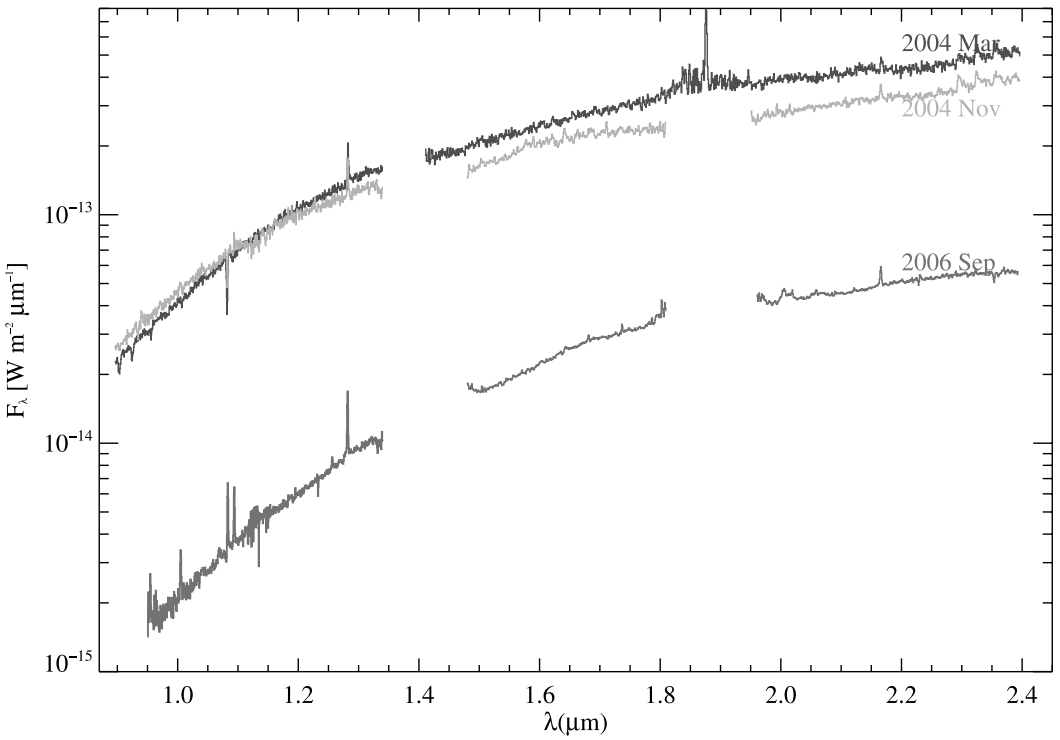

FIG. 4.—Flux-calibrated NIR spectra of V1647 Ori obtained with LIRIS on WHT. [*See the electronic edition of the Journal for a color version of this figure.*]

depressions can be seen around 2004 March 7 (JD 2,453,072) and 2004 April 12 (JD 2,453,108) in the light curves presented by Walter et al. (2004). Visual inspection suggests a possible periodicity in the light curve. In order to study this phenomenon quantitatively, a period search analysis was conducted, using the program package MUFRAN developed by Kolláth (1990).

The MUFRAN software is based on the Fourier transform. For a recent review of the time-series analysis of variable star data, see Templeton (2004 and references therein).

Our R_C and I_C data listed in Table 1 were supplemented with data taken from Semkov (2004, 2006) in the R_C and I_C filters. The imported data were zero-offset by 0.42 mag (R_C) and 0.17 mag (I_C), in order to reach a common average magnitude scale with our data. The most likely reason for such difference is the use of different methods to extract the stellar flux. Only the time interval between 2004 August 18 and 2005 February 11 (JD 2,453,235–JD 2,453,413) was considered, because outside this interval the longer timescale variation may falsify the result of the period analysis. Due to the evidence of a long-term brightness variation, allowance was made for the monotonous dimming: a straight line was fitted to each data set and subtracted to form magnitude differences with respect to this line.

The period search was performed separately for data in each photometric band. In the case of a finite data set and unevenly sampled data some false frequencies (aliasing) can appear in the Fourier power spectrum. These alias frequencies are centered on the real signals offset from those peaks, as indicated by the spectral window function of the Fourier transform. The temporal distribution of the photometric data of V1647 Ori is favorable, and the spectral window (see Fig. 6, *left*) indicates a negligible aliasing caused by the data sampling. Here we only show the spectral window function corresponding to the I_C filter data set, and note that the shape and the alias structure are practically the same in the case of the spectral window for the R_C data set. The power

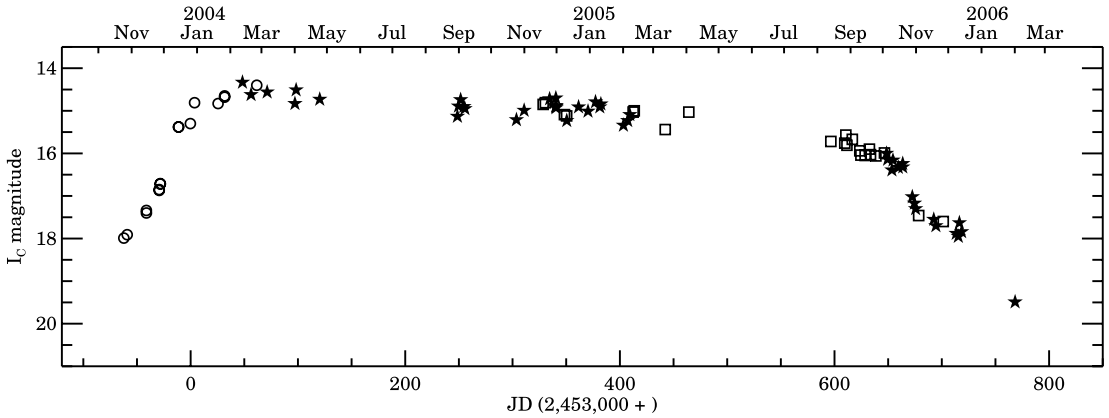

FIG. 5.—I_C-band light curve of V1647 Ori covering the complete 2 yr outburst period. *Stars*, Our observations reported in Table 1; *circles*, data from Briceño et al. (2004); *squares*, data from Ojha et al. (2006). The uncertainties are comparable with symbol sizes.

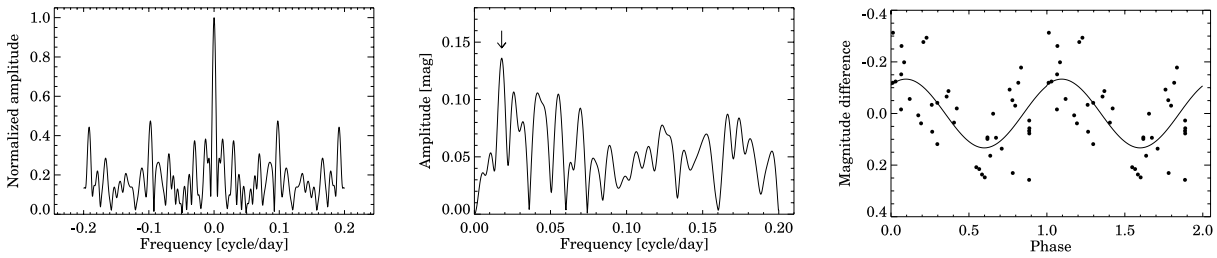

FIG. 6.—Results of the period search. *Left*: Spectral window function for the I_C photometric sample. *Middle*: Part of the Fourier power spectrum of the I_C data. The first high peak at the frequency of 0.0179 cycles day^{-1} corresponds to a period of 55.87 days. *Right*: I_C residual phase curve folded on the period of 55.87 days.

spectra typically contain a number of peaks (see Fig. 6, *middle*). We show in this figure only the lowest frequency part of the power spectrum; the rest of the power spectrum only contains much lower peaks than seen here. The highest peak appears at a frequency of $f = 0.0179$ cycles day^{-1} (equivalent to a period of 55.87 days) in the I_C data. The S/N is slightly above 3 in the region of the $f = 0.0179$ cycles day^{-1} peak, which gives significance to this peak. The S/N value was determined as the ratio of the amplitude of the main peak and the average amplitude present in the power spectrum after prewhitening with this frequency. Moreover, a peak can be considered as physically meaningful if it appears in the power spectra of each photometric observational series. The corresponding peak is situated at the frequency of 0.0163 cycles day^{-1} in the analysis of the shorter series of the R_C-filter data. The phase curve of the I_C residual photometric data folded on the 55.87 day period is shown in Figure 6 (*right*). The R_C-band folded light curve is qualitatively similar to that shown in Figure 6. It is worth mentioning that the negligible phase difference between the R_C and I_C folded light curves also implies a common origin of this periodicity. This means that the ~56 day periodicity is confirmed. We have plotted in Figure 7 the portion of the I_C light curve that was fitted with a sinusoidal curve plus a monotonic decrease. The time interval covered by our data is 200 days, which is only about four cycles of the possible period of 56 days. The periodic behavior is clearly seen in the curve, although a sinusoidal variation is regarded only as a first and crude approximation.

3.3. *Hour-Scale Variations*

Ojha et al. (2005) claimed weekly variations of the optical flux of V1647 Ori. Grosso et al. (2005) reported on a periodic variation in the X-ray flux of 0.72 days, about 17 hr. We have also searched for very short term variability in our optical data. We compared

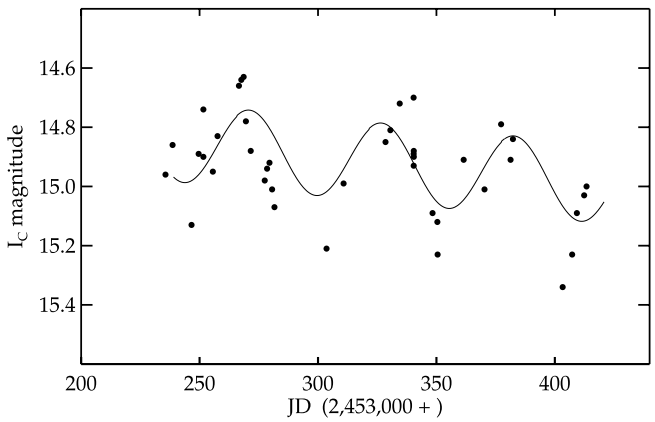

FIG. 7.—The I_C light curve with the fitted sinusoidal curve superposed. The dimming trend was also included. The quasi-periodic variation of the light curve is clearly detected.

five consecutive I_C-band observations of V1647 Ori obtained on the same night (2004 November 30) during a period of 2.5 hr with the 1 m RCC telescope. The first four measurements are identical within their formal photometric uncertainties (≈0.03 mag), but the fifth measurement deviates about 0.2 mag from the others. This value may be the characteristic variation expected on an hour scale.

3.4. *The Possible Origin of Variability*

In order to study further the mechanisms causing the initial brightening and the final fading, we plotted in Figure 8 optical and NIR color-magnitude diagrams, and looked for relationships between brightness and color-index variations. We also marked in Figure 8 the standard interstellar reddening law (Cohen et al. 1981).

Reipurth & Aspin (2004) noted that the star moved along the extinction path in the $J - H$ versus $H - K$ diagram during the initial brightening phase. Ojha et al. (2006) demonstrated that the final fading of the object in 2005 November also followed the same path in the opposite direction. However, the variation of the NIR and visible colors is not compatible with simple dust obscuration. It can be seen from Figure 8 that the amount of extinction needed to explain the color variation in the NIR is much larger than that required in the visible. In order to explain the amplitude of the outburst, a color-independent flux increase also has to be assumed. A similar conclusion was reached by McGehee et al. (2004).

In order to explain the flux variations during the plateau phase we looked at any possible relationship between brightness and color-index variations (Fig. 8). A loose trend that the star tends to be redder when dimmer can be observed in the diagrams. Eiroa et al. (2002) successfully explained the light variations of several young stars by obscuration by dense slabs within the circumstellar disk. Thus, obscuration by circumstellar dust structures orbiting at a distance of $R = 0.28(M/M_\odot)^{1/3}$ AU, implied by our ~56 day period, may explain at least part of the photometric variations during the plateau phase.

3.5. *Inclination of the Star-Nebula Axis Derived from the Brightness Evolution*

McNeil's Nebula shines due to the scattered light of V1647 Ori; therefore, its observed properties are closely related to the brightness of the star. Briceño et al. (2004) examined the temporal evolution of two well-defined positions of the nebula (marked as B and C in their Fig. 2), and concluded that their light curves followed the brightening of the star with delays of about 14 days (position B) and of more than 50 days (position C). The angular distance of 36″ between the star and position C implies a delay of 85 days. Since these delays carry information on the inclination of the nebula (see Fig. 9), we reanalyzed the three I_C-band light curves (from Fig. 3 in Briceño et al. 2004), supplemented with our measurements obtained in the period 2004 February–April,

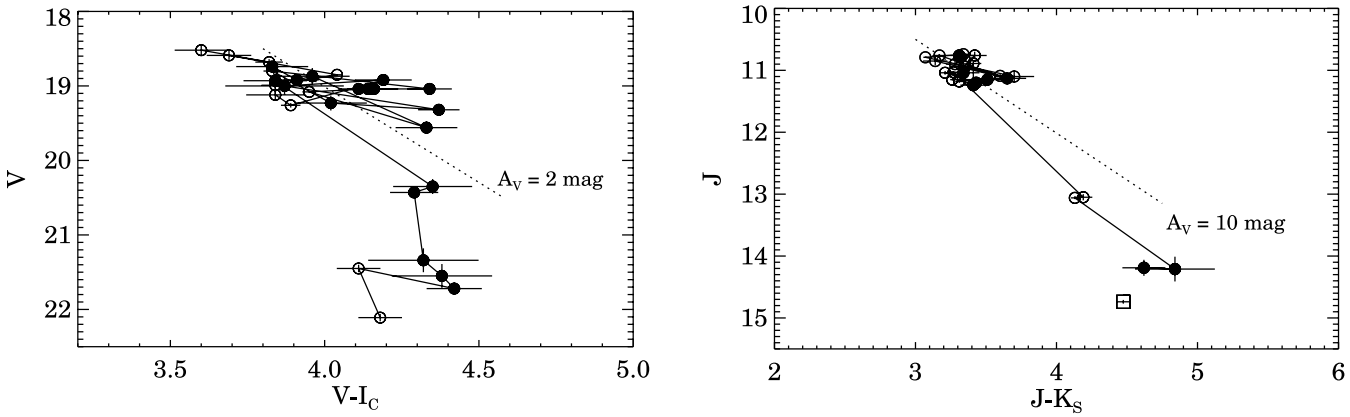

FIG. 8.—Relationship between the color indices and magnitudes of V1647 Ori during the monitoring period. *Left*, V vs. $V - I_C$; *right*, J vs. $J - K_s$. The filled symbols represent our measurements, and the open symbols are taken from Ojha et al. (2006). The dotted lines indicate the slope of the normal interstellar reddening (Cohen et al. 1981). Solid lines connect consecutive observed points.

in order to find the accurate time shifts between them. First, we interpolated the light curves for a sampling time of 0.25 days. The resulting light curves of V1647 Ori, position B, and position C are called A(t_i), B(t_i), and C(t_i), respectively, where t_i is the time ($i = 1. \ . \ . \ N$). Then we calculated a function called $D(s)$ as follows:

$$D(s) = \sum_{i=1}^{N} \mathrm{A}(t_i) - \mathrm{C}(t_i - s).$$

The quantity s that results in the lowest value of $D(s)$ gives the time shift between the light curves of A and C. The shifts between A and B can be calculated similarly. In this manner we obtained a time shift of 12.5 ± 2 days between V1647 Ori and position B and 50 ± 3 days between V1647 Ori and position C.

The measured time delay between the light curves of V1647 Ori and position C, together with the projected separation of the two objects, results in an angle of 61^{+3}_{-2} degrees between the axis of the nebula and the line of sight. Because the clump lies inside the polar stellar wind cavity of the star, this angle is a good estimate for the inclination of the rotation axis of the star (see Fig. 9). We estimated the uncertainty of the inclination derived this way as follows. We assumed that the Herbig-Haro object HH 23 (Eislöffel & Mundt 1997) lies exactly along the rotation axis of the star. Then

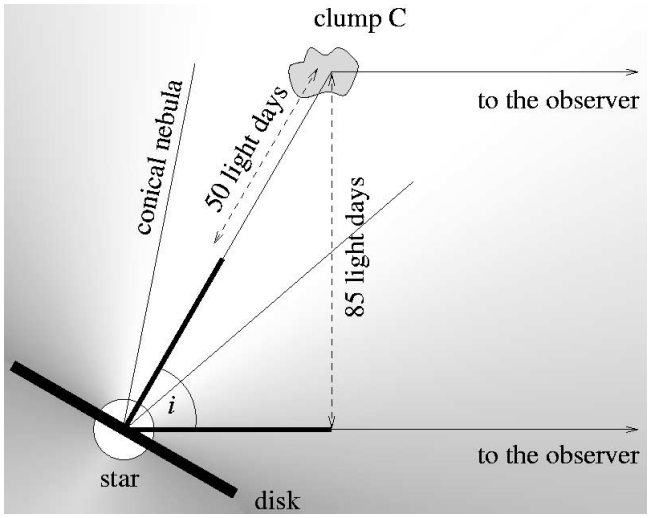

FIG. 9.—Geometry of McNeil's Nebula, deduced from the time delay between the light curves of V1647 Ori and clump C.

we assumed that the projected angle between the star–position C and star–HH 23 directions, 11°, is the same as the difference in their tilts to the line of sight. Thus, the total uncertainty of the inclination derived from the time delay of the brightness variation of clump C is ±14°.

The time delay between the light-curve features of V1647 Ori and position B results in $65^\circ \pm 8^\circ$. The inclinations derived from positions B and C are compatible within the errors. Due to the larger opening angle of the conical nebula at small distances from the star, position B is less suitable for estimating the inclination of the stellar rotation axis.

This result apparently conflicts with Rettig et al. (2005) finding that the disk of V1647 Ori is seen nearly face-on, because the absorption line of the cold CO due to the outer, flared regions of the disk cannot be observed in the high-resolution infrared spectrum of the star. But if the thickness H of the disk at a distance R from the star does not exceed $H/R \approx 0.50$, then the absorption lines produced by the outer disk is not expected to be observed in the spectrum of the star.

4. SPECTRAL EVOLUTION

Our NIR spectra, normalized to the continuum, are displayed in Figure 10 (*ZJ* band) and Figure 11 (*HK* band). The most prominent features are the Paβ, Paγ, and Brγ lines of H I in emission, the He I 1.083 μm line most of the time seen in absorption, the Mg I 1.50 μm line, and the rovibrational $\Delta\nu = +2$ transitions of CO at 2.3–2.4 μm in emission. These spectral features are present in all spectra, although significant changes can be recognized in the line strengths during our observational period of 30 months. In the following we analyze these spectral variations, including also data sets from Walter et al. (2004), Gibb et al. (2006), and Ojha et al. (2006) that cover shorter periods. We note that our last spectra were taken in 2006 May and September, when the outburst was over; thus, they are probably representative of the quiescent phase of the object.

Table 4 lists the equivalent widths and fluxes of the infrared lines. The NIR line fluxes were computed from the absolutely calibrated spectra, with a typical estimated uncertainty of about 15% in the brightest lines to 25% in the faintest ones. Figure 12 shows the time evolution of the line fluxes. In addition, we plotted the Hα and Ca II λ8542 lines, where line fluxes were derived by combining the equivalent widths published by Walter et al. (2004) and Ojha et al. (2006) and I_C and R_C magnitudes taken from Table 1 or from the literature for the same day as the spectroscopic data. The typical uncertainty of these latter flux values,

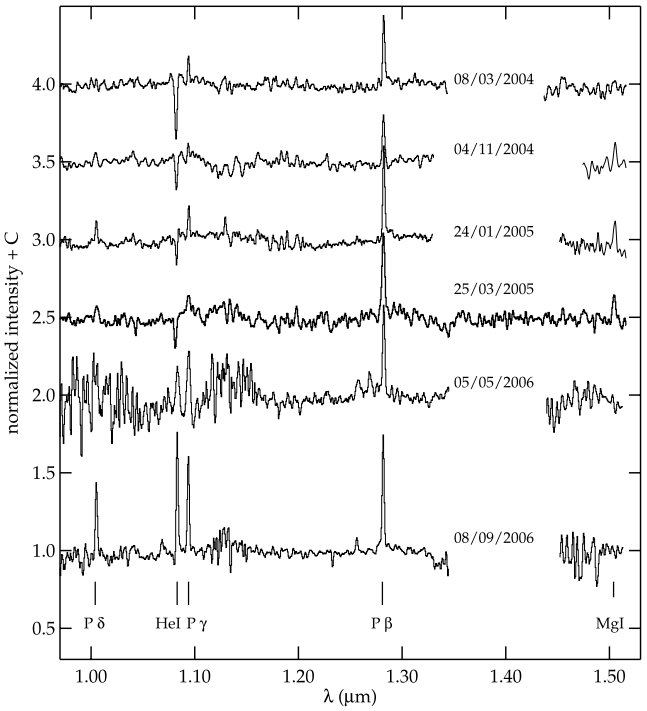

FIG. 10.—NIR (*ZJ* band) spectra of V1647 Ori obtained with LIRIS, normalized to the continuum.

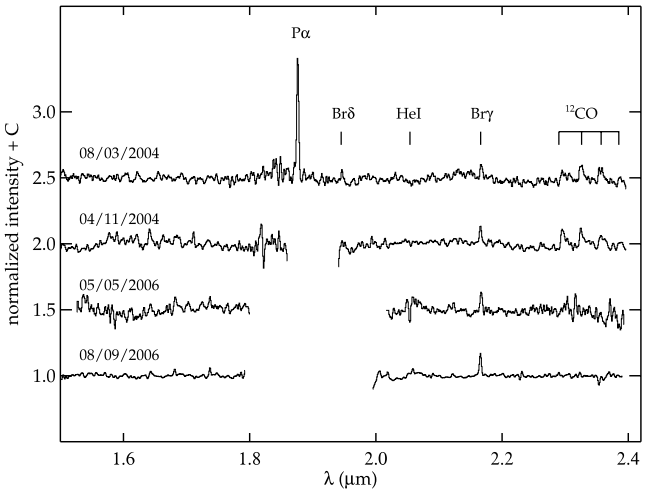

FIG. 11.—NIR (*HK* band) spectra of V1647 Ori obtained with LIRIS, normalized to the continuum.

derived from the errors of the magnitudes and equivalent widths, is about 6%. We noticed inconsistencies when comparing our line fluxes with those published by other authors for close observing dates. For this reason we recomputed their line fluxes combining the reported EW with photometric data. These are the values plotted in Figure 12.

4.1. *Hydrogen Lines*

Figure 12 shows that the line fluxes of Paβ, Brγ, and Hα declined slowly during the period of observation. The Paγ shows a similar trend, but with higher scatter.

In many young stellar objects the origin of H I lines is related to accretion processes. Muzerolle et al. (1998a) established empirical relationships between the accretion rate and the luminosity of Paβ and Brγ lines. The data in Figure 12 clearly indicate a parallel decrease of the strongest hydrogen emission lines during the whole outburst, which would suggest a decreasing accretion rate. Applying the relationships of Muzerolle et al. (1998a)—with the assumptions that V1647 Ori is located at 400 pc from the Sun, suffers an extinction of $A_V = 11$ mag, and has a mass of 0.5 $M_\odot$ and an accretion radius of 3 $R_\odot$—results in an accretion rate about 5×10^{-6} $M_\odot$ yr^{-1} in 2004 March, and a value an order of magnitude lower in 2006 May.

The Paschen lines of H I showed a P Cygni profile with a blueshifted absorption only in 2004 March, whereas the absorption part disappeared in later observations. Gibb et al. (2006) also reported the same variations in the profiles of the H I lines. Similar changes of the Hα and Ca II lines were reported by Ojha et al. (2006). These results indicate that at the beginning of the outburst the source of the H I lines was at least partly stellar wind, whose strength decreased during the outburst. As a consequence, the drop of accretion rate was probably smaller than we derived in the previous paragraph.

Walter et al. (2004) and Ojha et al. (2006) suggested a possible periodic behavior in the Hα equivalent width with a period of roughly 50 days. Since this period is similar to the one found in our I_C and R_C light curves (55.87 days; see § 3.2), it is tempting to speculate about a connection between the two cyclic phenomena. In order to check it, we folded all available Hα equivalent width data with the period of the optical light curve, and constructed a phase curve. It was found that the EW(Hα) and I_C values oscillate in opposite phase, i.e., the equivalent width of the Hα line is largest when the central object is dimmest. Since the equivalent width is the ratio of the true line flux to the continuum level, it is very likely that the periodic variations of the Hα EW are not intrinsic but due to the periodically changing continuum flux.

4.2. *Helium Lines*

The evolution of the He I 1.083 μm line tells an interesting story. It was seen in blueshifted absorption during the whole outburst, although its strength decreased with time (Fig. 12; see also Gibb et al. 2006). The flux decreases quickly toward the end of 2004, and later decreases again in 2006 May. In our spectra of 2006 May and September, taken in the quiescent phase, this line was detected *in emission*, without any apparent velocity shift (Fig. 10). The transition of the He I 1.083 μm line from absorption to emission is a remarkable event, not seen in any other line in our spectra. This line also shows a blueshifted ($\sim$500 km s^{-1}) absorption component in the spectrum taken in 2006 September.

In young stellar objects the He I 1.083 μm line is usually attributed to hot winds. The profile of the He I absorption line observed in V1647 Ori was similar to those seen in a large sample of strongly accreting T Tau stars (Edwards et al. 2006), where the whole velocity range of the He I wind can be observed against the stellar continuum. In these cases Edwards et al. (2006) argue that the wind traced by the He I 1.083 μm line originates close to the star and not from the inner part of the circumstellar disk. This may also be the case for the V1647 Ori system. The hard X-ray emission from V1647 Ori, observed by the X-ray observatories *Chandra* and *XMM-Newton* (Kastner et al. 2004; Grosso et al. 2005), indicates the presence of a magnetic reconnection ring located at 1–1.5 stellar radii above the stellar surface in the plane of the disk. We speculate that the source of the wind is the magnetic reconnection ring. This hypothesis is supported by the fact that the strongest He I line, observed on 2004 March 8 (Fig. 12; Vacca et al. 2004; Gibb et al. 2006), was preceded by a high X-ray emission event on 2004 March 7 (Kastner et al. 2004), indicating

TABLE 4
Equivalent Width and Flux of Near-Infrared Lines

Line	λ (μm)	2004 Mar		2004 Nov		2005 Jan		2005 Mar		2006 May		2006 Sep	
		EW	Flux	EW	Flux	EW	Flux	EW	Flux	EW	Flux	EW	Flux
Paδ	1.005	−0.8	1.2	−2.5	1.2	−2.1	0.5	−1.7	0.4	...	...	−12.4	0.26
He I	1.083	9.18	−5.9	4.3	−3.0	3.3	−1.1	5.2	−1.8	−11.6	0.3	−17.0	0.56
Paγ	1.094	−3.0	1.9	−2.4	1.7	−2.7	0.9	−2.2	0.8	−14.8	0.5	−13.4	0.50
Paβ	1.282	−10.7	14.4	−8.5	10.1	−12.5	8.1	−15.1	8.2	−14.9	1.4	−16.7	1.51
Mg I	1.504	−3.7	7.6	−2.8	4.4	−5.9	6.6	−6.7	5.2	...	...	−1.3	0.23
Brδ	1.945	−2.9	10.5	...	...	...	...	...	...	...	...	...	...
He I	2.058	< 0.8	< 3.0	0.8	−2.5	...	...	...	...	...	...	−1.7	0.77
Brγ	2.166	−5.2	22.0	−4.8	15.1	...	...	...	...	−6.9	4.0	−6.7	3.31

Note.—EW is in angstroms, and flux is in units of 10^{-17} Wm^{-2}.

a direct connection between the two phenomena. The drop of the flux of the He I 1.083 μm line during the outburst suggests weakening of the wind.

Edwards et al. (2006) proposed that there may be two types of the hot wind, producing absorption or emission of the He I 1.083 μm line. The transition of this line from absorption to emission at the end of the outburst indicates that the nature of the wind in V1647 Ori changed between the two types of hot wind.

We also detected the He I 2.058 μm line in absorption in both 2004 November and 2006 May. The apparent increase of its strength in the latter spectrum (taken during quiescence) is due to the lower continuum.

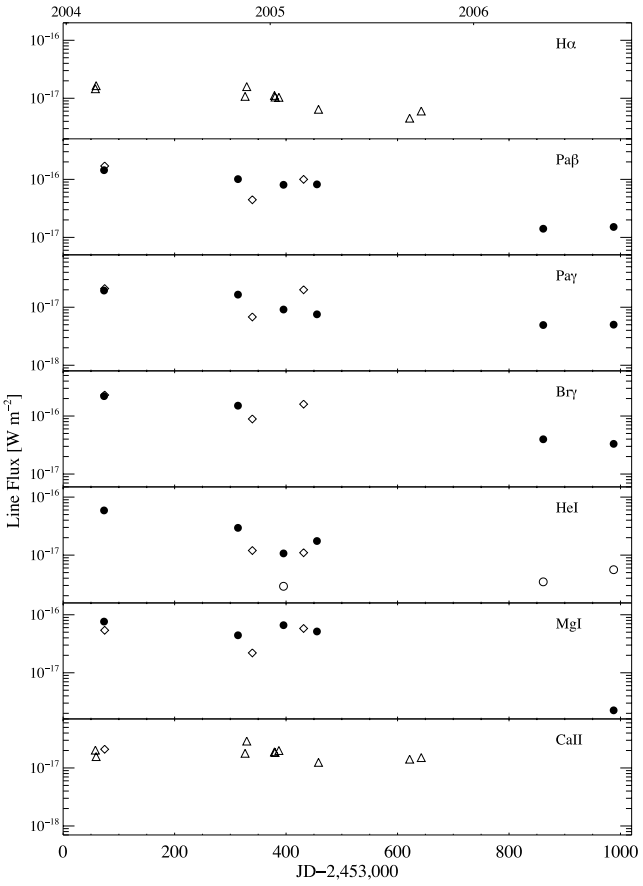

Fig. 12.—Flux evolution of NIR and optical spectral lines of V1647 Ori. *Circles*, This study, with open circles corresponding to the He I emission component (Table 4); *diamonds*, Gibb et al. (2006); *triangles*, Walter et al. (2004) and Ojha et al. (2006). The formal error bars are smaller than the symbol sizes.

4.3. *Other Spectral Features*

In Figure 12 we also plotted the flux of the Mg I 1.505 μm emission line. The feature was detectable during the whole outburst, showing hints for a slowly decreasing trend in flux. In the spectrum of 2006 May, during the quiescent phase, the line was not visible; the derived upper limit in Table 4 indicates that the Mg I 1.505 μm emission is weak in the quiescent phase.

The bottom panel of Figure 12 shows the flux variation of the Ca II λ8542 emission line based on literature data. This middle component of the Ca II triplet was found to be an excellent tracer of the accretion rate (Muzerolle et al. 1998b). It can be seen that, contrary to all the other lines in Figure 12, the flux of the Ca II λ8542 line was constant during the period of the observations (there is no available measurement from the quiescent phase). A reason for the discrepancy may be that the hydrogen and calcium lines originate from regions where the physical conditions are very different. Ojha et al. (2006) noted that the density of the Ca II region is very high and very optically thick. According to Muzerolle et al. (2001), optically thick lines are less reliable tracers of the variable accretion. The accretion rate, derived from its luminosity, is about $2 \times 10^{-6}\ M_{\odot}\ \mathrm{yr}^{-1}$, close to the values obtained from the hydrogen lines for the high state of the outburst.

The CO band head features at 2.3–2.4 μm were observed in strong emission during the whole outburst period (Fig. 11; see also Reipurth & Aspin 2004; Vacca et al. 2004; Rettig et al. 2005; Gibb et al. 2006). However, the CO feature is not present in our quiescent spectrum, suggesting that the appearance of this band is related to the outburst.

5. THE NEBULA AROUND V1647 ORI

McNeil's Nebula is a reflection nebulosity that scatters the light of its illuminating star, V1647 Ori. The optical and NIR morphology of the nebula can be seen in Figures 1 and 3, respectively. Their study provides information not only on the neighboring interstellar medium, but also on the outbursting star. In the following we describe the morphology of the nebula (see also Ojha et al. 2005; Reipurth & Aspin 2004).

Comparing the optical and NIR images, one immediately notices that the shape of the nebula looks rather different at optical (Fig. 1) and at infrared wavelengths (Fig. 3). In the optical images the nebula shows a conical shape, extending up to a distance of $\sim$50″ ($\sim$22,000 AU at the distance of the nebula) to the north. The diffuse emission area appears to be delimited by two bright regions indicating an opening angle of $\sim$50°. The northwestern side is marked by region B (named by Briceño et al. 2004), a plume located at a distance between 5″ and 10″. The northeastern rim appears more extended and is delimited by

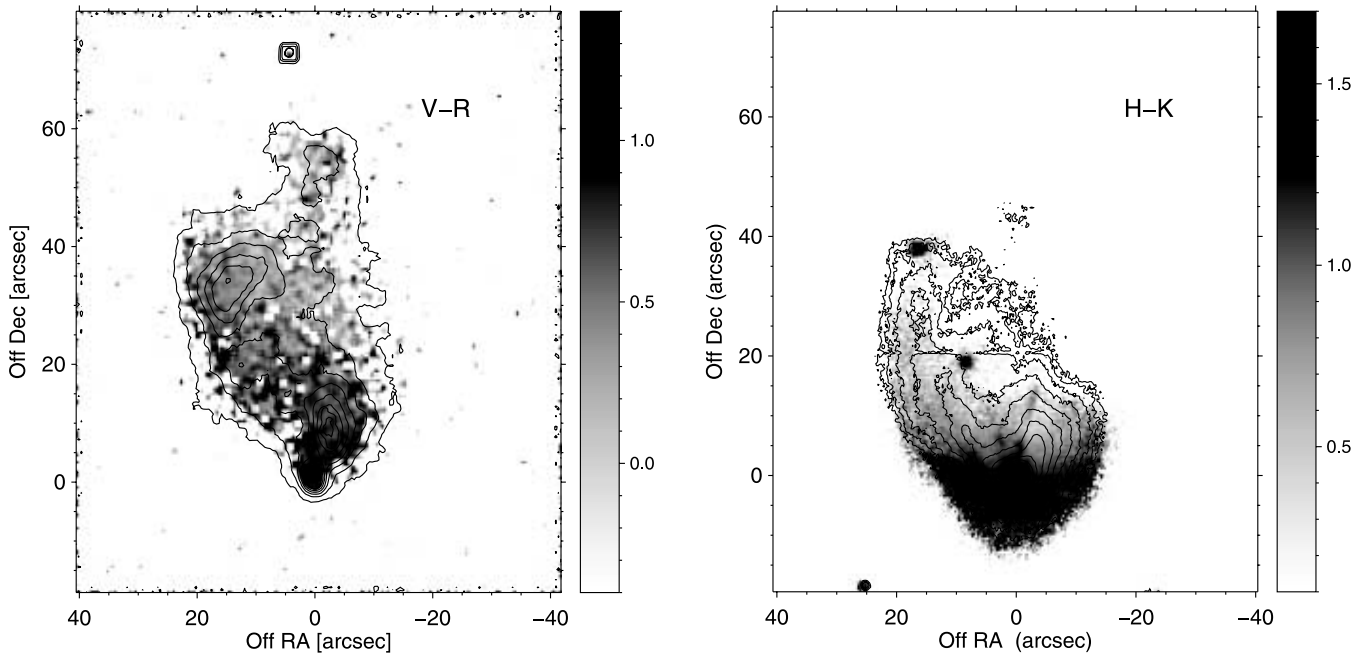

FIG. 13.—Color maps showing the $V - R_C$ (*left*) and $H - K_s$ (*right*) indices of the infrared nebula around V1647 Ori. The contours in the left and right panels represent the emission in the R_C and J bands, respectively. [*See the electronic edition of the Journal for a color version of this figure.*]

region C (also named by Briceño et al. 2004), which is located around 35″ from the star and is elongated perpendicularly to the radial axis from the star. No southern extension of the nebula can be recognized in the optical images.

In contrast to the optical, the infrared morphology indicates a much more compact structure, although the cometary shape can still be seen with a sharp curved tail along the northeastern side. The nebula appears to be more extended in the J band, exhibiting diffuse emission at both the northeastern and western sides. It appears roughly spherical in the K_s band, although the structure is flattened perpendicularly to the nebula axis; the largest size of the structure is ∼20″. This size corresponds to a diameter of ∼9000 AU at the distance of the Orion B cloud, which is slightly smaller than the size derived by Johnstone et al. (2001) for the matching submillimeter source Ori B N 55, about 13,500 AU. The southward extension is also clearly seen in the K_s band.

5.1. *Color Variations across the Nebula*

In Figure 13 we show the resulting optical ($V - R$) and NIR ($H - K$) maps. In addition, we obtained cross-cuts along the north-south direction passing through the star (Fig. 14).

Some distinguishable regions can be recognized in the $V - R_C$ map: (1) The bluest colors of the nebula are registered toward the northern end of the nebula, and its color is around $V - R_C \sim 0$ and $R_C - I_C \sim 0.3$ at 60″ from the star. Assuming that the light path along this direction is relatively cleaned of dust, we may observe the colors of the closest vicinity of the star, although somewhat modified by scattering and foreground extinction. These colors are very close to those of an intermediate A-type star, indicating the presence of a hot central area probably related to the outburst of this otherwise cold, late-type star (McGehee et al. 2004). (2) The plume located at a distance between 5″ and 10″ to the northwest (position B as defined by Briceño et al. 2004) appears redder than the rest of the nebula. (3) A compact region of strong reddening is observed toward the direction of V1647 Ori.

In the $H - K_s$ map the reddest part of the nebula can be seen to the south of the illuminating star, outlining a flattened D-shaped structure, whose elongation is nearly perpendicular to the axis of the optical nebula. The nebula appears very red along the east-west direction across the star ($J - H \sim 2$ and $H - K_s \sim 1$). When crossing the central part toward the north, the nebula changes rapidly to bluer colors ($J - H$ and $H - K_s \sim 0.5$), although the extension of the nebula is smaller than in the visible range. The infrared colors are redder at the south compared to the northern values at the same radial distance, indicating a larger extinction along the line of sight in the southern part, or part of emission from the dust envelope.

The observed color distributions of McNeil's Nebula can be interpreted in terms of a thick circumstellar envelope that intersects the light path from the central parts of the system to the scattering grains in the outer envelope. The envelope includes conical outflow cavities perpendicular to the disk plane, whose walls scatter the starlight. These cavities had been cleaned up by previous eruptions, and allow the light to escape and reach the northernmost regions of the nebula. The north-south asymmetry is likely caused by the inclination and the different amount of extinction along our line of sight. A similar geometry is assumed in theoretical models of infrared reflection nebulae around young stellar objects (Lazareff et al. 1990; Fischer et al. 1996).

5.2. *Extended Line Emission*

In Figure 15 (*left*) we present an emission-line Hα map, from which a properly scaled R-band image, obtained with the same camera, had been subtracted. The morphology observed in the [S II] line map is very similar, showing the same two major features around regions B and C. The [S II] emission at region C had already been reported by Eislöffel & Mundt (1997) during a quiescent period of V1647 Ori, and it is very likely associated with the object HH 22. We detected only knot A in our [S II] images; the other knots B to E are not seen, very likely because our images are not deep enough. The emission at ∼10″ north of V1647 Ori (region B) was not present in the [S II] map presented by Eislöffel

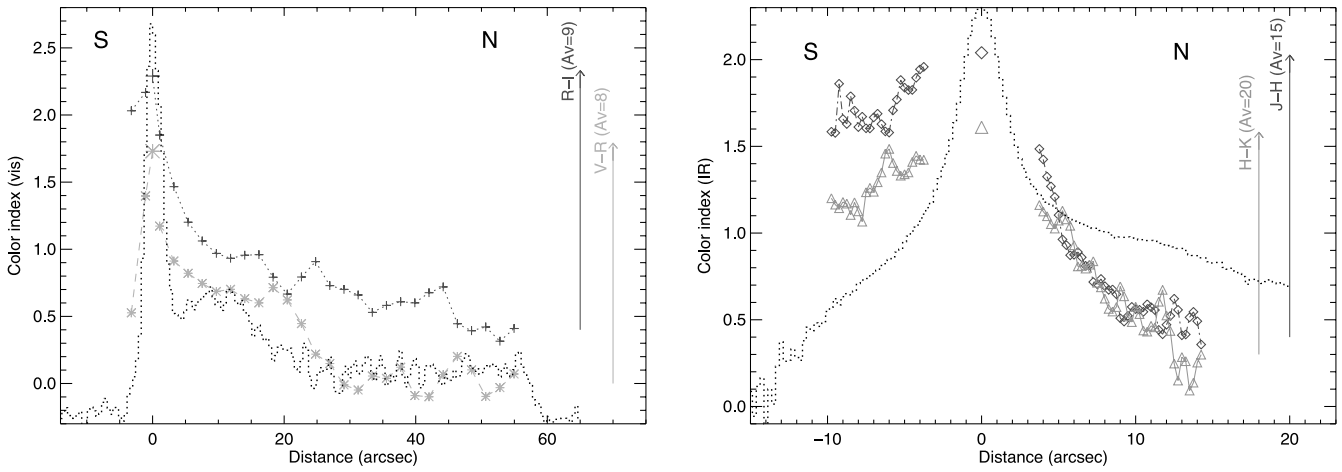

FIG. 14.—Different color profiles of the nebula along the north-south line, crossing the star. In the left panel we represent the variation of the $V - R_C$ (*stars*) and $R - I_C$ (*crosses*) colors, with the brightness profile as measured in the *R* band. In the right panel we represent the variation of the $J - H$ (*diamonds*) and $H - K_s$ (*triangles*) colors, with the brightness profile as measured in the *J* band. [*See the electronic edition of the Journal for a color version of this figure*.]

& Mundt (1997), and it can be associated with the outburst of our target.

We propose that the gas responsible for the emission of both Hα and [S II] is ionized by the hot radiation coming from the inner parts of the outburst region. In this scenario the density of the gas should not exceed the critical density of [S II] to avoid collisional deexcitation. Pure light reflection can be excluded, partly because the line-emitting area is less extended than the region observed in the adjacent continuum (e.g., the R_C or I_C band; see Fig. 15), and because optical spectra of the central part revealed Hα but not [S II] emission.

In Figure 15 (*right*) we display a region located north of McNeil's Nebula. The compact object seen at Δdecl. $\sim 160''$ corresponds to knot A of the object HH 23, according to Eislöffel & Mundt (1997). The object is clearly seen in the [S II] map, but is faint in Hα emission, indicative of shock excitation in this region. The source V1647 Ori was considered as the source of the HH 23 outflow by Eislöffel & Mundt (1997).

5.3. *Polarization Map*

NIR polarization measurements were obtained using LIRIS in the *J* band. The polarization vectors (their orientation and degree of polarization) are presented in Figure 16.

The general polarization pattern is centrosymmetric around V1647 Ori. The largest values of the polarization (slightly above 15%) are observed along the northeastern rim of the nebula and also, remarkably, to the southwest of the star. This distribution is consistent with dust scattering taking place in an outer envelope surrounding and obscuring the star. Region B, the northwestern plume close to the nucleus, shows no significant polarization. There is also a conspicuous lane of low polarization crossing the star from east to northwest, oriented almost perpendicularly to the direction of region C.

This pattern of polarization has been observed in other bipolar or cometary nebulae around young stellar objects (Tamura et al. 1991). It is usually attributed to the dusty disk surrounding the star, and it has been successfully simulated by Fischer et al. (1996).

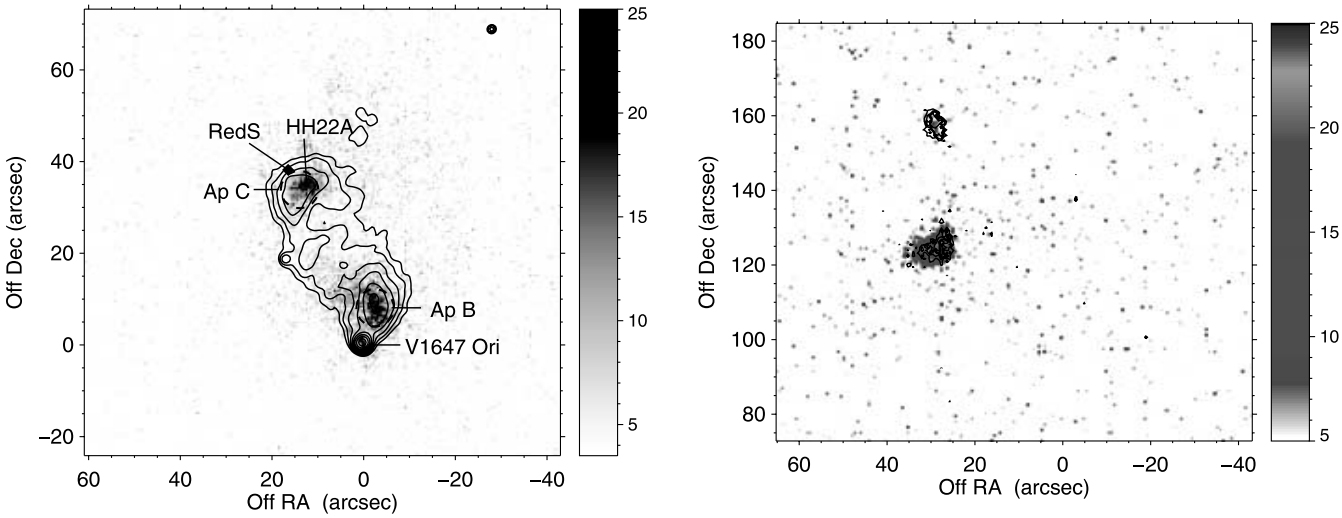

FIG. 15.—*Left*: Color-scale image corresponding to the Hα emission after continuum subtraction. The contour lines represent the emission in the R_C continuum. The filled diamond marks the position of the bright infrared source detected in our K_s band and also by Muzerolle et al. (2005) in *Spitzer* images. Apertures B and C from Briceño et al. (2004) are also indicated. *Right*: Color-scale image corresponding to the Hα emission in the region around the Herbig-Haro object HH 23. The contour lines represent the [S II] emission. Note the bright knot detected in [S II] emission at $\sim$160$''$ north, which appears very faint in the Hα band. The scale is twice that of the left panel. [*See the electronic edition of the Journal for a color version of this figure*.]

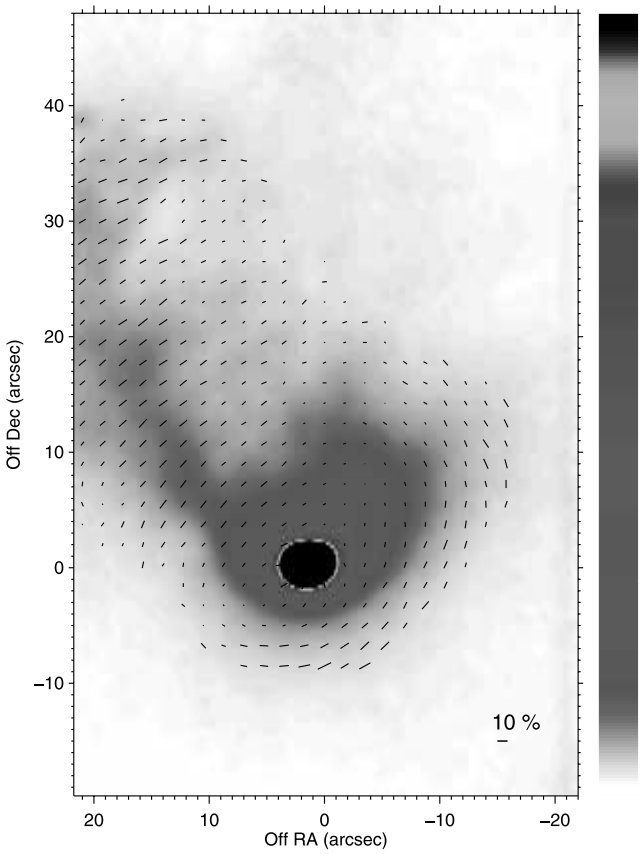

FIG. 16.—Polarization map obtained in the J band. The color-scaled image represents the total surface brightness distribution. [*See the electronic edition of the Journal for a color version of this figure.*]

A comparison with their simulations suggests that our observations are better explained with models that assume dust particles of 0.1–1 μm size. Among the different accretion disk types, our observations seem to be better reproduced by their SL model, which includes a massive self-gravitating disk in the form of an infinite isothermal slab (Lazareff et al. 1990). The polarization toward V1647 Ori (3.2% at P.A. = 140°) is also consistent both in value and orientation with the simulations by Fischer et al. (1996) for the same accretion disk type for the unresolved polarization.

5.4. *The Very Red Object Near HH 22*

Two bright red and compact sources appear in our K_s image (Fig. 3) toward the northeast of V1647 Ori. The two sources are roughly aligned with the star V1647 Ori. They are detected in all our K_s images obtained with LIRIS, even during the postoutburst phase when the brightness of V1647 Ori has decreased by more than 2 mag. These sources are not detected in our TCS images due to the poorer sensitivity of the camera. The closer source is located at the position $(\Delta\alpha, \Delta\delta) \simeq (8'', 19'')$. It was not detected in our J images and only barely detected in the H images. Its estimated magnitudes are $J > 19$, $H > 16$, and $K_s \simeq 15.0$. Given the uncertainties in the available data, we cannot say more about the nature of this object.

The farther source is located at an offset of $(\Delta\alpha, \Delta\delta) \simeq (16'', 38'')$. We estimate the following magnitudes for this source: $J > 19$, $H \gtrsim 16$, and $K_s \simeq 14.5$. We have checked the photometry of the source at different epochs, showing a variation smaller than 0.3 mag. This source has a corresponding entry in the 2MASS catalog (J05461423−0005261) whose measured magnitude is similar to ours ($\Delta K_s \simeq 0.4$) given the uncertainties inherent to the faintness of the source. Its NIR colors ($H - K_s \simeq 1.5$ and $J - H > 3$) are close to the locus of the classical T Tau stars (Meyer et al. 1997), although some reddening is also needed to bring its colors onto this locus. Muzerolle et al. (2005) detected an infrared source at 4.5 and 24 μm using the *Spitzer Space Telescope*. The position of this source, as overplotted in Figure 3, shows a perfect coincidence with the bright source in our K_s image. In the best-seeing images this source appears sligthly extended, as already noted by Muzerolle et al. (2005).

Muzerolle et al. (2005) claimed that this red object is part of the Herbig-Haro flow HH 22, and they propose to classify it as an extreme embedded class I source. In Figure 15 we overplotted the position of the red source using the coordinates given in Muzerolle et al. (2005) on our Hα emission-line map. It can be seen that the red source is located 3″–4″ north of the Hα emission-line region, which coincides with the position of knot A in HH 22 (Eislöffel & Mundt 1997). Thus, if the red *Spitzer* source is considered to be the driving source of HH 22, it should be explained why it is not aligned with the chain of the knots.

According to Briceño et al. (2004), the location of their region C is almost centered on the position of HH 22. The fact that region C brightened during the outburst could be explained by the overlap of two regions: one a dust cloud that reflects the brightening of the star, and the other related to HH 22 producing the line emission.

6. DISCUSSION

The eruptions of young stellar objects are commonly explained as a consequence of dramatically enhanced accretion from the circumstellar disk onto the star. Based on this idea, detailed models for FUors have been developed by Bell & Lin (1994; hereafter the BL model), which were later extended to include trigger mechanism for the eruption (Bell et al. 1995), and to take into account reprocessed light (Turner et al. 1997). In this section we first discuss whether the different types of observational results on V1647 Ori, collected during the 2 years of the outburst, could be consistently interpreted in the framework of the BL model. Then we comment on the question of whether V1647 Ori could be considered to be a member of either the FUor or the EXor group.

6.1. *The Outburst Mechanism*

6.1.1. *Preoutburst Phase*

In the BL model FUor eruptions occur in low-mass pre-main-sequence stars at an early evolutionary phase ($t_{\rm age} \leq 10^5$ yr). These young objects are still surrounded by an infalling envelope that feeds material onto an accretion disk. V1647 Ori seems to be precisely this type of star: based on preoutburst measurements, it is a class I/class II object ($t_{\rm age} \approx 10^4$ yr), whose flat spectral energy distribution (SED) shows that the object is deeply embedded (Ábrahám et al. 2004).

The rate at which material spirals within the disk toward the star is a critical input parameter of the BL model. If accretion exceeds a threshold value of about $5 \times 10^{-7}\ M_\odot\ {\rm yr}^{-1}$, then most of the matter would not fall directly onto the star due to the inefficient outward transportation of angular momentum. It piles up in the inner disk, soon or later leading to an outburst. In § 4 we determined the accretion rate of V1647 Ori from the Brγ line fluxes for 2006 May, when the star was in quiescent phase, and obtained a value of $5 \times 10^{-7}\ M_\odot\ {\rm yr}^{-1}$ (a similar figure was

proposed by Muzerolle et al. 2005). The result agrees with the threshold value, indicating that V1647 Ori just passed the criterion of the BL model to produce an outburst, but its accretion rate in the disk was probably the lowest among all known FUors.

6.1.2. *The Outburst*

According to the BL model, the inflowing matter piles up in the inner disk at $R_{\rm limit} \approx 0.25$ AU, until its column density—and thus opacity—becomes high enough to switch on a thermal instability. An ionization front propagates in the inner disk, and the emission of the bright ionized region behind the front causes the increase of flux at optical and NIR wavelengths. V1647 Ori brightened by about 4.5 mag in the $I_{\rm C}$ band, which is a typical value for FUor eruptions. One should note, however, that the brightening of V1647 Ori consisted of two effects of comparable amplitude: an intrinsic brightening presumably related to the appearance of a new hot component in the system (probably the ionized inner disk), and a dust-clearing event that reduced the extinction along the line of sight (Reipurth & Aspin 2004; McGehee et al. 2004). Thus, the amplitude of the outburst of V1647 Ori was probably lower than is typical of FUors. Also, the bolometric luminosity increased only by a factor of 15, in contrast with the factor of $\sim$100 of classical FUors. Concerning the hypothesis of the BL model that matter piles up at $R_{\rm limit}$, it is interesting to recall that in § 3 we speculated that the periodic optical dimming could be the consequence of variable extinction due to obscuration by a dense circumstellar dust clump orbiting the star. The period of the optical variability of 56 days implies an orbital radius of $R = 0.28\ (M/M_{\odot})^{1/3}$ AU, which is close to the expected $R_{\rm limit}$ of the inner disk where material piles up, suggesting that the extinction might be related to this reservoir of matter.

During the outburst the high temperature in the ionized part of inner disk leads to higher efficiency of angular momentum transport, resulting in dramatically increased accretion rate onto the star. Muzerolle et al. (2005) determined that the accretion rate increased by a factor of 15. In § 4 we calculated an accretion rate of $5 \times 10^{-6}\ M_{\odot}\ {\rm yr}^{-1}$ from the Brγ line luminosity for the peak of the outburst (close to the estimates of Vacca et al. [2004] and Gibb et al. [2006]). These results suggest that in the eruption of V1647 Ori both the peak value of the accretion rate and its increase with respect to the quiescent phase were relatively modest compared to those of other FUors.

Many observations indicated that a new, hot component appeared in the V1647 Ori system during the outburst. This component is probably the inner ionized part of the disk, for which the BL model predicts a surface temperature of 6000–8000 K. The observations seem to be consistent with this expectation: McGehee et al. (2004) attempted to fit the SED of this new component with a 7000 K blackbody; Muzerolle et al. (2005) assumed a temperature of 6000 K for the innermost, outbursting part of the disk; and the disk model of Ábrahám et al. (2006) predicted a temperature of 4200 K for the same part. The high temperature of the inner disk is also supported by the CO excitation diagrams (2400 K; Rettig et al. 2005). It is also consistent with the model of Bell & Lin (1994) that the region participating in the outburst is limited to within a few AU around the star (see the interferometric measurements by Ábrahám et al. [2006] and the estimations of Tsukagoshi et al. [2005]).

The main apparent contradiction to the BL model is related to the timescales. In their standard self-regulated model, Bell & Lin (1994) computed a rise time of several decades (matching the case of the FUor V1515 Cyg). In order to explain shorter initial brightening curves (e.g., V1057 Cyg and FU Ori), they proposed "triggered eruption," by which means a nearby companion can temporarily increase the accretion rate. V1647 Ori went into outburst in about 4 months (Briceño et al. 2004); thus, it is tempting to speculate on such a trigger mechanism, but so far there is no observational signature of any companion. One can realize, however, that in the BL model all timescales depend on the accretion rate in the outer disk: lowering the accretion rate leads to shorter eruptions. Thus, the very low accretion rate of V1647 Ori (practically at the threshold value for producing an outburst) can be one factor to explain the short initial brightening. Table 2 in Bell & Lin (1994) presents rise-time estimates for several $\dot{M}_{\rm in}$ values. Interpolating within this table suggests, however, that the resulting timescales are still too long for V1647 Ori. The other main factor that determines the timescale of the initial brightening is the viscosity parameter in the outburst high state of the inner disk α_h. Working again from the numbers of Table 2 of Bell & Lin (1994) we concluded that a value of $\alpha_h = 3 \times 10^{-2}$ (rather than their standard value of $\alpha_h = 10^{-3}$) would produce the observed rising timescale of about 4 months.

6.1.3. *The Plateau Phase*

The initial brightening of V1647 Ori was followed by a 2 yr long slow fading. This is the period under which the inner disk depletes and the matter becomes neutral again. The length of this period is determined by the same viscosity parameter as we discussed in relation to the length of the initial brightening. It is encouraging that, adopting again $\alpha_h = 3 \times 10^{-2}$ and taking into account the low accretion rate of V1647 Ori, from the numbers in Table 2 of Bell & Lin (1994) we estimated a plateau phase of about 2 yr, consistent with the observations.

According to the model of Bell & Lin (1994), the fading is due to the decreasing accretion rate. Checking two independent indicators of the accretion rate, in § 4 we found the somewhat contradictory result that the temporal evolution of the flux of the H I lines indeed shows such a monotonic drop in the accretion rate, while the Ca II λ8542 line fluxes remained constant during the whole outburst.

The fading rate during this plateau was about 0.04 mag yr^{-1}. As mentioned already in § 3.1, the fact that the fading rate appears wavelength-independent suggests that no significant temperature variation occurred in the inner parts of the star-disk system in this period.

6.1.4. *Final Fading*

In 2005 October, V1647 Ori started a sudden fading that took approximately 4 months and ended when the object returned to the quiescent, preoutburst state at optical and NIR wavelengths. Remarkably, the rate of the brightness change was similar during the final fading and the initial brightening. This is a natural fact in the BL model, where the ionization front reverses at the end of the outburst and proceeds with the same speed as in the extension phase. We note that such a return of a FUor to the quiescent phase has never been observed before.

6.1.5. *Recurrent Outbursts?*

Following an eruption, steady accretion from the outer disk slowly fills up the inner disk at $R_{\rm limit}$, and the system is prepared for a new outburst. The timescale between outbursts is determined by the viscosity parameter of the model in the quiescent cold state of the system α_C. From a rough interpolation in Table 2 of Bell & Lin (1994), one may conclude that $\alpha_C \approx 1.5 \times 10^{-3}$ would produce the 40 yr period between the last and the present outburst of V1647 Ori. This number is larger than the corresponding value in the standard BL model by a factor of 15.

6.1.6. *Dust Sublimation/Condensation*

Similarly to the initial brightening, the final fading also consisted of two events: an intrinsic fading and an increasing extinction along the line of sight. This suggests that the effects changing the extinction must be reversible. This reversibility is also supported by the fact that V1647 Ori already had an outburst in 1966–1967 (Aspin et al. 2006). Thus, among the possible mechanisms responsible for the dust-clearing event, sublimation of dust particles at the beginning of the outburst is a likely explanation. It could be a reversible process, since the increasing extinction observed during the final fading can be due to the condensation of dust grains (dust condensation effects were already observed in young eruptive stars, e.g., V1515 Cyg in 1980; see Kenyon et al. 1991).

6.1.7. *Wind*

The analysis of spectral lines (§ 4) suggests the presence of a wind that was strongest at the peak of the outburst. During the plateau phase the P Cygni profile of the prominent spectral lines disappeared, also indicating that the strong wind present at the peak of the outburst decreased considerably. Such a wind is not included in the model of Bell & Lin (1994) but should be taken into account for a detailed modeling of V1647 Ori. The detailed model should also take into account the interesting finding that the He I absorption turned into emission in the quiescent phase, indicating that the type of the wind changed after the end of the outburst.

6.1.8. *Conclusions*

From the comparison of observations of V1647 Ori with the model of Bell & Lin (1994), we conclude that the BL model reproduces most observational results, but in order to match the timescales 1 order of magnitude higher viscosity parameters—in both the cold and the high states—have to be assumed. The physical reason behind the increased viscosity parameter cannot be deduced from the available data.

6.2. *FUor or EXor?*

In the literature there is an ongoing debate on the classification of V1647 Ori, presenting a number of arguments supporting either the FUor- or the EXor-like nature. On the one hand, in our previous paper (Ábrahám et al. 2004) we argued that the shape of the SED is similar to those of FUors, and now we can add that the model of Bell & Lin (1994) developed for explaining the FUor phenomenon can model the outburst of V1647 Ori reasonably well. On the other hand, the short timescale of the eruption (2 yr) and the recurrent nature argue more for an EXor-type event. EXors, however, are assumed to be classical T Tau stars, while V1647 Ori is obviously in an earlier evolutionary phase than T Tau stars. We speculate that V1647 Ori, together with another recently erupted young stellar object OO Serpentis (Kóspál et al. 2006), might form a new class of young eruptive stars. Members of this class may be defined by their relatively short timescales, recurrent outbursts, modest increase in bolometric luminosity and accretion rate, and an evolutionary state earlier than that of typical EXors.

7. SUMMARY

Comparison of our optical and NIR data obtained in 2004 February–2006 September on V1647 Ori with published results led to the following new results: (1) The brightness of V1647 Ori stayed more than 4 mag above the preoutburst level until 2005 October, when it started a rapid fading. (2) In the high state we found a periodic component in the optical light curves with a period of 56 days. (3) The time delay between the brightness variations of the star and a nebular position corresponds to an angle of $61^\circ \pm 14^\circ$ between the axis of the nebula and the line of sight. (4) The overall appearance of the infrared and optical spectra did not change in the period 2004 March–2005 March, although a steady decrease of H I emission-line fluxes could be observed. We show that the periodic variations of the Hα equivalent width, suggested by several authors, could be caused by variation of the continuum with the 56 day period. In 2006 May, in the quiescent phase, the He I 1.083 μm line was in emission, contrary to its deep blueshifted absorption observed during the outburst. (5) The $J - H$ and $H - K_s$ color maps of the infrared nebula reveal an envelope around the star whose largest extension is about 18″ (0.03 pc). (6) The color distribution of the infrared nebula suggests reddening of the scattered light inside a thick circumstellar disk. (7) Comparison of the K_s and Hα images of McNeil's Nebula shows that HH 22A, the *Spitzer* infrared source, and the bright clump C of the nebula may be unrelated objects. (8) We show that the observed properties of V1647 Ori could be interpreted in the framework of the thermal instability models of Bell et al. (1995). (9) We speculate that V1647 Ori might belong to a new class of young eruptive stars, defined by relatively short timescales, recurrent outbursts, modest increase in bolometric luminosity and accretion rate, and an evolutionary state earlier than that of typical EXors.

Financial support from the Hungarian OTKA grants K62304, T42509, and T49082 is acknowledged. A. M., J. A.-P., M. C.-L., and M. J. V.-N. acknowledge support from grant AYA 2001-1658, financed by the Spanish Dirección General de Investigación. Many thanks are due to Maria J. Arevalo, Gabriel Gómez, José A. Caballero, and Fernanda Artigue for helping with the data collection at the IAC-80 and TCS telescopes. We also thank Nicola Caon for his continuous help with all IRAF-related questions. This project has been supported by the Australian Research Council. L. L. K. is supported by a University of Sydney Postdoctoral Research Fellowship.

APPENDIX

THE 2MASS SOURCE J05461162−0006279

The object located at about 30″ west and 30″ south of V1647 Ori (Fig. 3) can be identified with the 2MASS source J05461162−0006279. The source is very red, as shown by its appearance as a remarkably bright object in *Spitzer* images at 4.5 and 24 μm (Muzerolle et al. 2005). It was also detected by *XMM-Newton* (Grosso et al. 2005); however, it remains undetected in optical images. Thanks to the excellent seeing (0.65″) during the night 2004 November 4, we could resolve this target into two components separated by 1.2″, oriented along the east-west axis (see Fig. 3). The magnitude of each component was obtained by performing PSF photometry using the DAOPHOT package in IRAF. The primary star is the western component, and has $J = 14.14$ and $K_s = 11.43$; the secondary star has $J = 15.72$ and $K_s = 13.79$. The color index $J - K_s$ is 2.7 and 1.9 for the primary and secondary stars, respectively. These color indices are redder than those of normal M stars according to Bessell & Brett (1988), suggesting the possibility that this double system is also embedded in the Orion B molecular cloud.

REFERENCES

Ábrahám, P., Kóspál, Á., Csizmadia, S., Moór, A., Kun, M., & Stringfellow, G. 2004, A&A, 419, L39
Ábrahám, P., Mosoni, L., Henning, T., Kóspál, Á., Leinert, C., Quanz, S. P., & Ratzka, T. 2006, A&A, 449, L13
Acosta-Pulido, J. A., et al. 2003, ING Newsl., 7, 15
Andrews, S. M., Rothberg, B., & Simon, T. 2004, ApJ, 610, L45
Aspin, C., Barbieri, C., Boschi, F., diMille, F., Rampazzi, F., Reipurth, B., & Tsvetkov, M. 2006, AJ, 132, 1298
Bell, K. R., & Lin, D. N. C. 1994, ApJ, 427, 987
Bell, K. R., Lin, D. N. C., Hartmann, L. W., & Kenyon, S. J. 1995, ApJ, 444, 376
Bessell, M. S., & Brett, J. M. 1988, PASP, 100, 1134
Briceño, C., et al. 2004, ApJ, 606, L123
Cohen, J. G., Frogel, J. A., Persson, S. E., & Elias, J. H. 1981, ApJ, 249, 481
Cutri, R. M., et al. 2003, The IRSA 2MASS All-Sky Point-Source Catalog (Pasadena: Caltech), http://irsa.ipac.caltech.edu/applications/Gator
Edwards, S., Fischer, W., Hillenbrand, L. A., & Kwan, J. 2006, ApJ, 646, 319
Eiroa, C., et al. 2002, A&A, 384, 1038
Eislöffel, J., & Mundt, R. 1997, AJ, 114, 280
Fischer, O., Henning, T., & Yorke, H. W. 1996, A&A, 308, 863
Gibb, E. L., Rettig, T. W., Brittain, S. D., Wasikowski, D., Simon, T., Vacca, W., Cushing, M. C., & Kulesa, C. 2006, ApJ, 641, 383
Grosso, N., et al. 2005, A&A, 438, 159
Hamilton, C. M., et al.. 2005, AJ, 130, 1896
Johnstone, D., Fich, M., Mitchell, G. F., & Moriarty-Schieven, G. 2001, ApJ, 559, 307
Kastner, J. H., et al. 2004, Nature, 430, 429
———. 2006, ApJ, 648, L43
Kenyon, S. J., & Hartmann, L. 1991, ApJ, 383, 664
Kenyon, S. J., Hartmann, L. W., & Kolotilov, E. A. 1991, PASP, 103, 1069
Kolláth, Z. 1990, The Program Package MUFRAN (Budapest: Konkoly Obs.), http://www.konkoly.hu/Mitteilungen/muf.tex
Kóspál, Á., Ábrahám, P., Acosta-Pulido, J., Csizmadia, S., Eredics, M., Kun, M., & Rácz, M. 2005, Inf. Bull. Variable Stars 5661
Kóspál, Á., et al. 2006, A&A, submitted
Lazareff, B., Pudritz, R. E., & Monin, J.-L. 1990, ApJ, 358, 170
Manchado-Torres, A., et al. 2003, Proc. SPIE, 4841, 160
McGehee, P. M., Smith, J. A., Henden, A., Richmond, M., Knapp, G. R., Finkbeiner, D., & Ivezic, Z. 2004, ApJ, 616, 1058
McNeil, J. W. 2004, IAU Circ. 8284
Meyer, M. R., Calvet, N., & Hillenbrand, L. A. 1997, AJ, 114, 288
Muzerolle, J., Calvet, N., & Hartmann, L. 2001, ApJ, 550, 944
Muzerolle, J., Hartmann, L., & Calvet, N. 1998a, AJ, 116, 2965
———. 1998b, ApJ, 492, 743
Muzerolle, J., Megeath, S. T., Flaherty, K. M., Gordon, K. D., Rieke, G. H., Young, E. T., & Lada, C. J. 2005, ApJ, 620, L107
Ojha, D. K., et al. 2005, PASJ, 57, 203
———. 2006, MNRAS, 368, 825
Oliva, E. 1997, A&AS, 123, 589
Reipurth, B., & Aspin, C. 2004, ApJ, 606, L119
Rettig, T. W., Brittain, S. D., Gibb, E. L., Simon, T., & Kulesa, C. 2005, ApJ, 626, 245
Semkov, E. 2004, Inf. Bull. Variable Stars 5578
———. 2006, Inf. Bull. Variable Stars 5683
Serra-Ricart, M., Oscoz, A., Sanchis, T., Mediavilla, E., Goicoechea, L. J., Licandro, J., Alcalde, D., & Gil-Merino, R. 1999, ApJ, 526, 40
Stetson, P. B. 1987, PASP, 99, 191
Tamura, M., Gatley, I., Joyce, R. R., Ueno, M., Suto, H., & Sekiguchi, M. 1991, ApJ, 378, 611
Templeton, M. 2004, J. AAVSO, 32, 41
Tsukagoshi, T., Kitamura, Y., Kawabe, R., Saito, M., Yokogawa, S., & Kurono, Y. 2005, PASJ, 57, L21
Turner, N. J. J., Bodenheimer, P., & Bell, K. R. 1997, ApJ, 480, 754
Vacca, W. D., Cushing, M. C., & Rayner, J. T. 2003, PASP, 115, 389
Vacca, W. D., Cushing, M. C., & Simon, T. 2004, ApJ, 609, L29
Walter, F. M., Stringfellow, G. S., Sherry, W. H., & Pollatou, A. F. 2004, AJ, 128, 1872